

Using OSSEs to Evaluate GXS Impact in the Context of International Coordination

ERICA L. MCGRATH-SPANGLER,^{a,b} N. C. PRIVÉ,^{a,b} BRYAN M. KARPOWICZ,^{b,c} ISAAC MORADI,^{b,d}
AND ANDREW K. HEIDINGER^e

^a Morgan State University, Baltimore, Maryland

^b NASA Global Modeling and Assimilation Office, Greenbelt, Maryland

^c University of Maryland, Baltimore County, Baltimore, Maryland

^d Earth System Science Interdisciplinary Center, University of Maryland, College Park, College Park, Maryland

^e GeoXO Program Office, NOAA/NESDIS/Center for Satellite Applications and Research, Madison, Wisconsin

(Manuscript received 23 October 2023, in final form 22 January 2024, accepted 8 February 2024)

ABSTRACT: The Geostationary Extended Observations (GeoXO) program plans to include a hyperspectral infrared (IR) sounder on its central satellite, expected to launch in the mid-2030s. As part of the follow-on to the GOES program, the NOAA/NASA GeoXO Sounder (GXS) instrument will join several international counterparts in a geostationary orbit. In preparation, the NASA Global Modeling and Assimilation Office (GMAO) assessed the potential effectiveness of GXS both as a single GEO IR sounder and as part of a global ring that includes international partners. Using a global observing system simulation experiment (OSSE) framework, GXS was assessed from a numerical weather prediction (NWP) perspective. Evaluation of the ability of GXS, both alone and as part of a global ring of GEO sounders, to improve weather prediction of thermodynamic variables was performed globally and regionally. GXS dominated regional analysis and forecast improvements and contributed significantly to global increases in forecast skill relative to a Control. However, more sustained global improvements, on the order of 4 days, relied on international partnerships. Additionally, GXS showed the capability to improve hurricane forecast track errors on the time scales necessary for evacuation warnings. The FSOI metric over CONUS showed that the GXS observations provided the largest radiance impact on the moist energy error norm reduction. The high-temporal-resolution atmospheric profile information over much of the Western Hemisphere from GXS provides an opportunity to improve the representation of weather systems and their forecasts.

SIGNIFICANCE STATEMENT: NOAA and NASA are currently planning the GeoXO mission as a follow-on to the GOES program. As part of this process, NASA's Global Modeling and Assimilation Office has performed several experiments using an observing system simulation experiment (OSSE) framework to assess the potential impact of the GeoXO Sounder (GXS) on numerical weather prediction within the context of international partners launching similar instruments. As part of this assessment, it was found that assimilation of GXS data has the ability to improve both the model analyzed weather and forecasts of the weather, specifically over the domain that GXS observes. Global improvements relied more heavily on a solution consisting of multiple instruments to form a global ring.


KEYWORDS: Atmosphere; Atmospheric profilers; Satellite observations; Soundings; Numerical weather prediction/forecasting; Data assimilation

1. Introduction

In recent decades, the utility of hyperspectral infrared (IR) sounders in the understanding of atmospheric processes, constituents, and numerical weather prediction (NWP) has been well established (e.g., McNally et al. 2006; Chahine et al. 2006; McCarty et al. 2009; Pagano et al. 2010; Reale et al. 2018; Wells et al. 2020; McGrath-Spangler et al. 2021; Ganeshan et al. 2022; Coopmann et al. 2022; McGrath-Spangler et al. 2022). IR radiance data from low-Earth orbit (LEO) have been widely available from the Atmospheric Infrared Sounder (AIRS) on board the National Aeronautics and Space Administration's

(NASA) *Aqua* satellite, the Cross-Track Infrared Sounder (CrIS) on board the *Suomi NPP* and the *National Oceanic and Atmospheric Administration 20 and 21* (NOAA-20 and NOAA-21) satellites and the Infrared Atmospheric Sounding Interferometers (IASI) on board the European Space Agency's (ESA) *MetOp* satellites and have been successfully assimilated into NWP data assimilation systems. Although providing key high-vertical-resolution temperature and water vapor information to NWP systems, LEO sounders are limited horizontally and temporally (McCarty et al. 2021). These limitations make observations in cloudy atmospheres, the monitoring of rapidly evolving phenomena, and processes with a diurnal cycle difficult (Schmit et al. 2009; Iturbide-Sanchez et al. 2022) and may negatively affect stakeholders.

These shortcomings are addressed by the proposed launch of hyperspectral IR sounders into geostationary orbit. This proven concept was originally developed by NASA for the Geosynchronous Imaging Fourier Transform Spectrometer (GIFTS) mission concept (Zhou et al. 2002; Velden et al. 2005)

 Denotes content that is immediately available upon publication as open access.

Corresponding author: Erica L. McGrath-Spangler, erica.l.mcgrath-spangler@nasa.gov

DOI: 10.1175/JTECH-D-23-0141.1

© 2024 American Meteorological Society. This published article is licensed under the terms of the default AMS reuse license. For information regarding reuse of this content and general copyright information, consult the AMS Copyright Policy (www.ametsoc.org/PUBSReuseLicenses).

Brought to you by NOAA Central Library | Unauthenticated | Downloaded 08/29/24 03:48 PM UTC

and successfully implemented with the launch by the China Meteorological Administration's (CMA) Geosynchronous Interferometric Infrared Sounder (GIIRS) on board the *Fengyun-4A* (FY-4A) and *Fengyun-4B* (FY-4B) satellites, launched in December 2016 and June 2021, respectively (Yang et al. 2017; Niu et al. 2023). GIIRS thus provides the first geostationary Fourier transform spectrometer radiances with a high-temporal-resolution suitable for NWP (Guo et al. 2021).

Following this success, the European Organisation for the Exploitation of Meteorological Satellites (EUMETSAT) has proposed the launch of the Meteosat Third Generation (MTG) hyperspectral infrared sounder (IRS) for late 2024 or early 2025 (Holmlund et al. 2021; Coopmann et al. 2023). MTG-IRS will be the first geostationary hyperspectral IR instrument providing full disk coverage and will do so in two spectral bands (longwave and midwave infrared) at a spatial resolution of 4 km at satellite subpoint (Holmlund et al. 2021). Furthermore, the Japan Meteorological Agency (JMA) plans to expand their Himawari follow on program (Himawari-10) to include a hyperspectral infrared sounder from geostationary orbit [Geostationary Himawari Sounder (GHMS)] in the 2029 time frame, the first such instrument from Japan (Okamoto et al. 2020; Bessho et al. 2021). In the United States, NOAA and NASA are collaborating on the Geostationary Extended Observations (GeoXO) program to include a hyperspectral IR sounder, to be positioned at 105°W (McGrath-Spangler et al. 2022; Iturbide-Sanchez et al. 2022). This international collaboration will enable meeting the World Meteorological Organization's (WMO) goal of a global "ring" of geostationary hyperspectral IR observations (WMO 2019). In an attempt to better understand the impact of such observations, Li et al. (2022) provides a general overview of applications of geostationary hyperspectral IR radiance data, summarizing the work of Jones et al. (2017), Okamoto et al. (2020), and Wang et al. (2021), among others who found improvements from the assimilation of data from geostationary IR observations.

The approach used here is a set of observing system simulation experiments (OSSEs). This is an independent methodology for the evaluation of proposed instrument systems (e.g., Atlas et al. 1985; Arnold and Dey 1986; Errico et al. 2013; Hoffman and Atlas 2016). This cost-effective approach allows testing of new, hypothetical instruments without an existing dataset to assess the impact of the new instrument and provide an estimate of the associated uncertainty in an NWP context. In addition, this allows an optimization of the observing strategy and enables rapid assimilation upon deployment.

Here, a set of global, NWP OSSEs is used to evaluate the impacts of the proposed GeoXO Sounder (GXS) as both an independent geostationary IR instrument and as part of a larger global ring of such instruments. To ensure realistic performance, NASA's Global Modeling and Assimilation Office (GMAO) has developed and extensively validated the OSSE framework used here (Errico et al. 2013; Privé et al. 2021; El Akkraoui et al. 2023; Privé et al. 2023). Previously, this framework has been used to successfully evaluate the impact of supplemental rawinsondes (Privé et al. 2014), atmospheric motion vectors and infrared radiances (McCarty et al. 2021),

radio occultations (Privé et al. 2022), and an earlier evaluation of GXS within a global ring of four geostationary IR sounders (McGrath-Spangler et al. 2022).

This article is organized as follows. A description of the GeoXO program, and GXS in particular, is provided in section 2. Section 3 describes the OSSE framework and the data assimilation system used. Experimental design is discussed in section 4 and the results are provided in section 5. Section 6 contains a summary and the conclusions.

2. Description of GeoXO sounder

NOAA's current geostationary satellite program, the Geostationary Operational Environmental Satellites R (GOES-R) series of satellites, is expected to operate through the mid-2030s. The current capabilities of the GOES-R series include advanced imaging, lightning mapping, space weather monitoring, and solar imaging, among others. In preparation for the next generation of spaceborne observations from geostationary orbit, NOAA and NASA are developing the GeoXO constellation to provide continuity of observations of Earth's weather and environment that meet national environmental sensing requirements (Pearlman et al. 2022).

Among the proposed improvements, GeoXO will increase spatial resolution of observations from visible and IR imagery and lightning mapping. Additional proposed capabilities that will be new with the GeoXO program include ocean color imagery, atmospheric composition measurements, and infrared sounding. The hyperspectral atmospheric composition and infrared sounding instruments, as well as a partner payload, will be mounted on a new, centrally located satellite at approximately 105°W.

The proposed GXS, consistent with current hyperspectral sounders from LEO orbit, measures atmospheric radiation in thousands of spectral channels, providing a high vertical sounding of the atmosphere necessary for weather forecasting (Schmit et al. 2009). These channels provide information on temperature, water vapor, and trace gases, thus providing insight into many atmospheric processes and as such are critical to improving forecasts from NWP systems.

The benefit of these observations from a geostationary orbit include the enhanced temporal resolution, capable of overcoming many limitations of IR sounders from LEO orbit (Jones et al. 2017; Li et al. 2018; Wang et al. 2021). Additionally, GXS will have a horizontal resolution of about 4 km, providing a higher spatial resolution than is currently available from LEO hyperspectral sounders (Iturbide-Sanchez et al. 2022). These advantages will allow the ability to observe gaps between clouds, and weather system development and the associated processes. There are also nowcasting applications from GXS information (Schmit et al. 2009). Furthermore, with a lower data latency and more rapid assimilation of critical data into NWP systems, there is an opportunity to improve atmospheric forecasts (Noh et al. 2020). A description of the configuration and feasibility of the proposed GeoXO Sounder and its ground processing system is available in Iturbide-Sanchez et al. (2022).

3. OSSE configuration

A traditional OSSE system consists of three main components, specifically, 1) a Nature Run (NR), 2) a data assimilation system (DAS) and forward model to conduct the experiments, and 3) global observations simulated from the NR that statistically resemble real observations from existing instruments. The OSSE system used by NASA's GMAO has been verified to ensure robust performance through rigorous testing (e.g., Errico et al. 2013; Errico and Privé 2018; Privé et al. 2023) to provide an understanding of the global impact of proposed instruments relevant to NWP. In particular, the response of the OSSE system to simulated hyperspectral IR instruments well mimics the response of the semioperational system used by the GMAO (McGrath-Spangler et al. 2022).

Gelaro et al. (2015) describes the well-validated NR used by the GMAO, the G5NR. G5NR is a 2-yr free-running integration of the Goddard Earth Observing System (GEOS) (Rienecker et al. 2008) atmospheric general circulation model (AGCM) with a horizontal resolution of approximately 7 km and 72 vertical levels from the surface to 0.01 hPa. With a temporal resolution of 30 min, the simulation begins 1 May 2005, although the free-running model does not represent the real weather for that period. Instead, it is statistically consistent with the physical atmosphere and is considered to be the “truth” from which observations are simulated and against which experiment analyses and forecasts are evaluated. An advantage of a traditional OSSE is that since the truth is completely known, errors may be explicitly calculated.

The DAS used for the experiments is a more modern version of the GEOS (Molod et al. 2015) than was used to compute the NR, combined with the Gridpoint Statistical Interpolation (GSI) (Wu et al. 2002; Kleist et al. 2009). Running on a cubed sphere dynamical grid (Lin 2004; Putman and Lin 2007), the experiments have a spatial resolution of C360 (approximately 0.25°) and 72 vertical layers transitioning from terrain following near the surface to pure pressure levels aloft. A baseline run, similar to that described by Privé et al. (2023) was used for the calculation of the background error for the hybrid four-dimensional ensemble variational (4D-EnVar) assimilation scheme (Todling and El Akkraoui 2018) to reduce computational expense. The Community Radiative Transfer Model (CRTM) (Han et al. 2006; Chen et al. 2008; Ding et al. 2011; Johnson et al. 2023) was used to assimilate satellite radiances.

Although this is considered to be a “fraternal twin” setup, multiple modifications were made to maximize differences between the G5NR and the GEOS DAS used for the experiments in order to maximize the observation impact realism in the OSSE. Notably, a two-moment microphysics convection scheme described by Barahona et al. (2014) was used in place of the default single moment (Bacmeister et al. 2006) used in the G5NR. This change is most significant in highly convective regions of the tropics and midlatitudes of the summer hemisphere. An adjustment to the relative humidity threshold and a different boundary layer parameterization, which impact estimates of the inversion height, are additional changes meant to introduce model error between the NR and the

DAS model in an attempt to better mimic model errors when assimilating real observations and to minimize the suboptimality of the “fraternal twin” setup (Privé and Errico 2013).

The DAS used here has been updated since the results of McGrath-Spangler et al. (2022), reducing the degree of “twinning” further. Details of this update, including changes to the model and DAS, may be found in Privé et al. (2023). This is significant for several reasons. The model has evolved further, introducing additional differences between the model used to generate the NR and that in the DAS used to compute the OSSE experiments. This provides additional differences upon which the observations may provide information and produces more error that can be reduced by their assimilation.

The observing system has been updated from one resembling the system available in 2015 to one resembling 2020. This update allows a more realistic measurement of the potential impact of future observations beyond current capabilities. Although the COVID-19 pandemic resulted in a decrease in the number of aircraft observations available in 2020, Ingleby et al. (2021) showed that the decrease in forecast skill was largely insignificant. The largest impact was in the upper troposphere of the Northern Hemisphere (250–200 hPa, the level of aircraft cruising altitudes) and most of the impact came from the loss of aircraft winds rather than temperatures. The OSSE framework has been extended to include the month of September, allowing a longer time period to evaluate and additional atmospheric processes that may be investigated, namely, Atlantic hurricanes, which are more prevalent in the month of September in the NR than in the months evaluated in the previous work (Reale et al. 2017).

Simulated observations were generated by sampling the Nature Run at the spatiotemporal locations of actual observations from June to September 2020, consistent with the procedure of Errico et al. (2017). An exception was made for August AIRS observations due to a failure of the instrument. These were taken from the spatiotemporal locations of August 2021 observations. This approach is to mimic the observing system available in 2020. A list of the observations assimilated in the OSSE Control is available in Table 1, and a spatial distribution is shown for a 6-h assimilation window in Fig. 1 from the OSSE, consistent with the OSSE time. Observations not included are GOES radiances and those sensitive to stratospheric ozone as they produce minimal impact in the GMAO OSSE framework. The different methods described in Errico et al. (2017) were used to generate each observation type from the NR. For the distribution of the assimilated observations to reflect the atmospheric state of the NR, the radiance data types are affected by the cloud fields of the NR for quality-control purposes and use CRTM in their simulation.

Correlated and uncorrelated errors are added to the synthetic observations assimilated in the Control experiment to provide an approximation of the real errors that originate from instrument errors, representativeness errors, and errors in the data assimilation system's process of handling observations. Simulated observations tend to have lower intrinsic error than real observations, so this is done, customized to the

TABLE 1. List of observations assimilated in the control.

Instrument type	Instrument
Conventional	Radiosonde, surface, and aircraft
Ground retrieved	NEXRAD winds and wind profilers
Satellite retrieved	Geostationary AMV SEVIRI (<i>Meteosat-10</i> ; <i>Meteosat-8</i>) AHI (<i>Himawari-8</i>) GOES Imager (<i>GOES-16</i> ; <i>GOES-17</i>)
	Polar AMV MODIS (<i>EOS Terra</i> ; <i>EOS Aqua</i>)
	Scatterometer ASCAT (<i>MetOp-A</i>)
	Radio occultation bending angle
Satellite radiance	Infrared IASI (<i>MetOp-A</i> ; <i>MetOp-B</i>) CrIS FSR (<i>SNPP</i> ; <i>NOAA-20</i>) AIRS (<i>EOS Aqua</i>)
	Microwave temperature AMSU-A (<i>NOAA-15</i> ; <i>NOAA-18</i> ; <i>NOAA-19</i> ; <i>MetOp-B</i> ; <i>MetOp-C</i> ; <i>EOS Aqua</i>) ATMS (<i>SNPP</i> ; <i>NOAA-20</i>) SSMIS (<i>F17</i>)
	Microwave humidity MHS (<i>MetOp-B</i> ; <i>MetOp-C</i>) ATMS (<i>SNPP</i> ; <i>NOAA-20</i>) AMSR-2 (<i>GCOM-W1</i>) GMI (<i>GPM</i>)

instrument type, to statistically resemble the magnitude and correlation scale of real observation errors.

In addition to the observations assimilated in the Control, hyperspectral infrared observations from GXS and two other geostationary locations (approximately those of MTG-S and Himawari-10) were generated following the methodology

described in McGrath-Spangler et al. (2022). Although an in-depth discussion of their generation is described in that work, a brief description is provided here. All three geostationary instruments were simulated identically, the only difference being the satellite subpoint.

Hourly observations were simulated for GXS (satellite subpoint of 105°W) and at satellite subpoints of 0° and 140°E with a spectral wavenumber resolution of 0.625 cm⁻¹ for a range from 680 to 2250 cm⁻¹. In practice, however, observations were not assimilated with an hourly temporal frequency for global NWP. Observation locations were generated based on the coverage from GOES-R and relocated to the appropriate satellite subpoints. They were then interpolated from the G5NR to the corresponding spatiotemporal locations. Cloud contamination was accounted for using probabilistic methods (Errico et al. 2017) and the high-resolution IR radiances were partially thinned with cloud contaminated data preferentially discarded. However, unaffected radiances that peak above low-lying clouds were retained. The spatial distribution of the GEO IR observations is available in Fig. 1 and for quality-controlled GEO IR observations from a surface sensitive channel in Fig. 2.

The channel selection used here is identical to that of McGrath-Spangler et al. (2022) with the exception that channels outside the range of GXS are discarded here. Fifty-three temperature sounding channels, ranging from 680 to 980 cm⁻¹, and 15 water vapor channels, ranging from 1765 to 2005 cm⁻¹, were assimilated by the GEOS DAS. This channel selection balances the minimization of interchannel correlations while preserving a high vertical resolution of the atmosphere, providing profiles of atmospheric phenomena. Most hyperspectral infrared instruments use a similar procedure (McNally et al. 2006; McCarty et al. 2009; Reale et al. 2018; McCarty et al. 2021). The optimal selection of channels

Observations in GMAO's GEOS

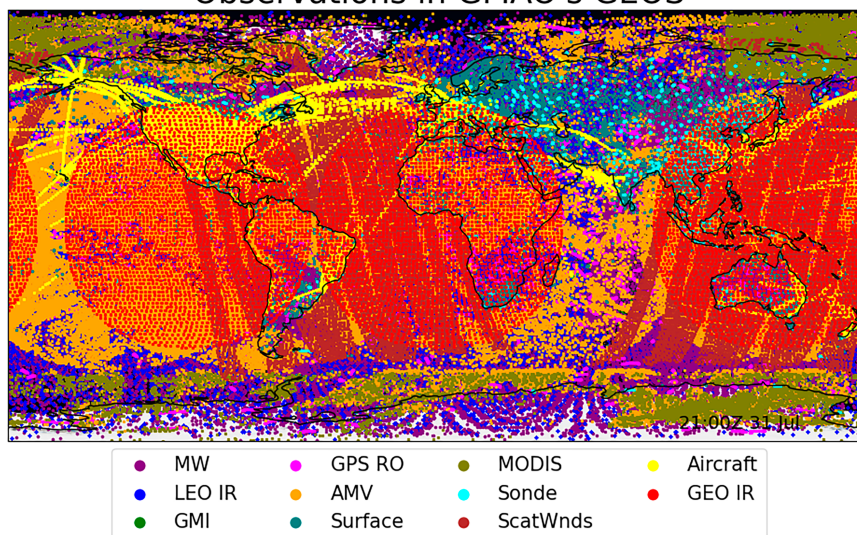


FIG. 1. All observation types assimilated in the OSSE for a 6-h period centered on OSSE time 0000 UTC 1 Aug 2006 before quality control. The geostationary IR observations are indicated in red.

Quality Controlled GEO IR Observations

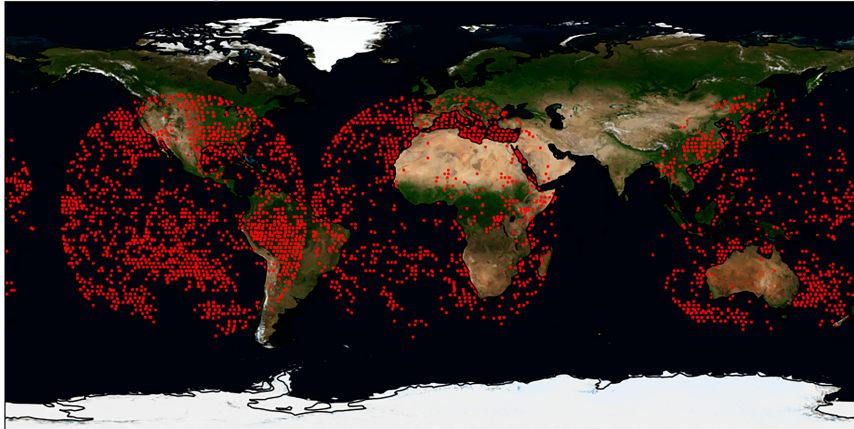


FIG. 2. As in Fig. 1, but for only the quality-controlled geostationary IR sounder observations. The observations are plotted for GEO IR channel 107, corresponding to 716.25 cm^{-1} .

is an active area of research [Coopmann et al. \(2022\)](#) and it is expected that the channel selection will be different once the instrument becomes operational. It is also important to note that the advantages of a hyperspectral IR sounder extend beyond NWP applications to include, among others, observational constraints for atmospheric constituents, and a geostationary IR sounder will allow near-real-time, high-vertical-resolution observations of rapidly evolving weather phenomena relevant to human activities.

As in [McGrath-Spangler et al. \(2022\)](#), errors were not explicitly added to the geostationary hyperspectral IR radiances for several reasons. Primarily, the error magnitude of the proposed instruments is currently unknown since the instrumentation is still in development and its estimate is uncertain. However, implicit error exists due to several issues, including some representativeness error since the high-resolution G5NR and the DAS used for assimilation consist of different resolutions. [Errico et al. \(2017\)](#) contains more general information about observation generation and the associated errors.

4. Experiment design

A set of OSSE experiments consists of a control run and permutations of that control in order to assess the impact of a proposed instrument with the control run serving as a baseline for comparison. For the OSSE set described here, the assimilated observations in the Control are listed in [Table 1](#). Two permutations were computed. The first is the GXS-Only run that assimilated all of the Control observations plus simulated observations consistent with the proposed GXS instrument. The second is the Global Ring experiment that again assimilated all observations in the Control, plus geostationary hyperspectral IR observations consistent with the satellite subpoints of GXS, MTG-IRS, and GHMS. Thus, the only differences between GXS-Only and Global Ring are the additions of GEO IR sounders at the positions of MTG-IRS and Himawari-10 GHMS.

A multiweek period was used to spin up the radiance bias coefficients and background state during the calibration process. This iterative process was separate from the experiment

spinup with the purpose of adjusting the OSSE system to mimic the real system. All experiments simulated the period 1 July–30 September 2006 with a spinup period for GEO IR starting 26 June. However, the OSSE system itself benefited from several months of calibration to adjust the bias correction coefficients ([Privé et al. 2023](#)) and initial conditions were selected at the end of this process. The analysis was generated at C360 horizontal resolution on the cubed sphere grid (approximately $0.25^\circ \times 0.3125^\circ$) using a 6-h assimilation window and a hybrid 4DEnVar assimilation scheme ([Todling and El Akkraoui 2018](#)). Ten-day forecasts, initialized at 0000 UTC from 1 July to 30 September 2006, were run at the same C360 resolution as the analysis. The simulated errors and cloud probability functions were adjusted to statistically resemble existing observations in the real world.

Aside from the satellite subpoint used in defining the location of the observations, the three geostationary hyperspectral IR sounders are identical in terms of radiance channels. The GEOS hybrid 4DEnVar assimilation scheme used by the GEOS DAS uses a 6-h temporal thinning box. The GEO IR observations were therefore assimilated in a 6-h assimilation window and thus did not make optimal temporal use of the GeoXO observations. Horizontal thinning used a 180-km thinning box, consistent with IR sensors from polar-orbiting satellites. Since a 6-h assimilation window is used by the GSI, the temporal frequency of the assimilated data is lower than the hourly observations. The GSI performed cloud detection consistent with the methodology of [Eyre and Menzel \(1989\)](#). The assimilation procedure used to perform variational bias correction on the GEO IR radiances and observation errors is consistent with the procedure for other infrared satellite radiances.

5. Results

Assimilation of a new instrument may affect the performance of an experiment in multiple ways, necessitating evaluation of several performance measures. Here, results are

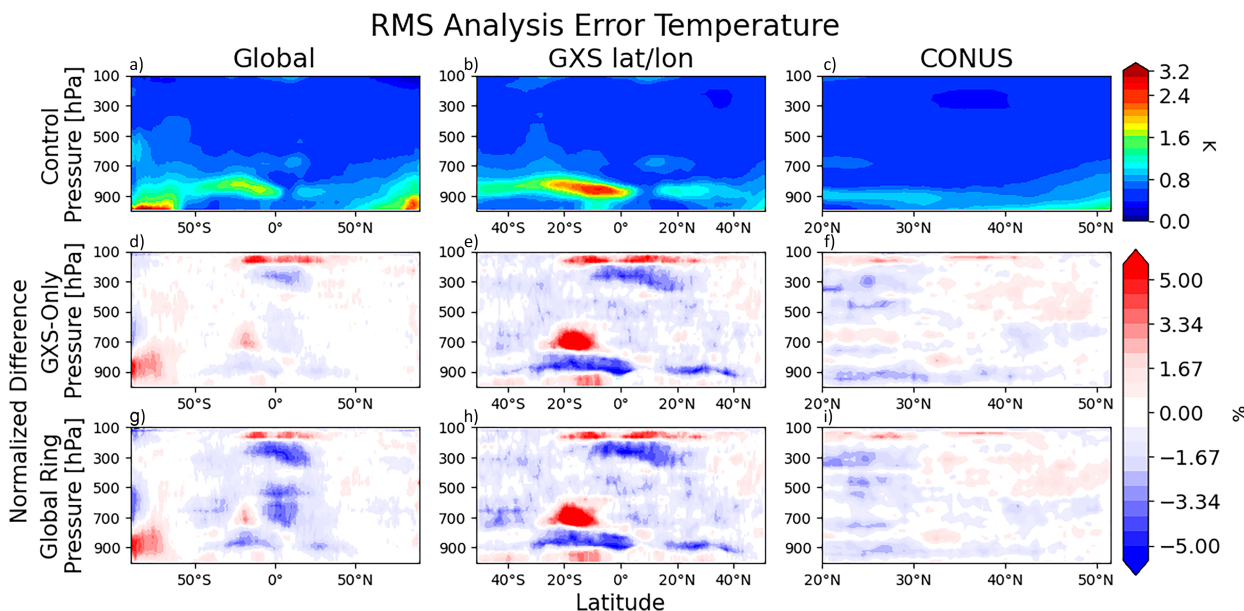


FIG. 3. Zonal (a)–(c) RMSE for temperature (K) in the Control vs the nature run, (d)–(f) the normalized change in RMSE (%) relative to the Control in the GXS-Only experiment, and (g)–(i) the normalized change in RMSE (%) relative to the Control in the Global Ring experiment for the (left) global, (center) GXS-defined latitudes and longitudes, and (right) CONUS regions. In the difference plots, blue or red indicates an improvement or degradation, respectively, by the addition of the geostationary IR radiances.

shown from the assimilation of geostationary hyperspectral IR radiances in four categories. The first evaluates the impact on the analysis. These analyses affect the initial conditions for the NWP forecasts, which are examined in the second category. Third, the impact of geostationary IR assimilation on hurricane representation is described. Fourth, the forecast sensitivity of observation impact (FSOI) metric (Langland and Baker 2004; Zhu and Gelaro 2008; Gelaro and Zhu 2009) is described for both global and contiguous United States (CONUS) domains.

a. Analysis

In a traditional OSSE, the “truth” is perfectly known since it is determined by the nature run. This allows the computation of errors directly and exactly, aside from differences in resolution. Here, the nature run is used in the computation of the analysis error over the duration of the experiments, from 1 July to 30 September. Evaluation of changes to the analysis error are particularly consequential because the analysis is used in the initialization of forecasts and these errors are subsequently passed to the results of the NWP models.

Figure 3 shows the root-mean-square temperature error of the Control and the normalized differences of the GXS-Only and Global Ring experiments relative to the Control. For this and subsequent figures, the root-mean-square error (RMSE) is computed over three domains, global, GXS latitude/longitude, and CONUS. The GXS domain is defined by the latitudes and longitudes approximately observed by the simulated GXS instrument in these experiments (156°–54°W longitude and equatorward of 51°N/S). The CONUS domain is defined as between 130° and 60°W longitude and between 20° and 52°N latitude.

In the Control, much of the temperature error is in the lower troposphere, below approximately 700 hPa. In the global domain, the largest error is at the poles and an elevated arc of enhanced error from the equator toward Antarctica is associated with the low cloud deck west of South America. This feature is emphasized within the GXS domain, which has a greater fractional areal coverage of the responsible cloud deck. The CONUS domain, which is north of the cloud deck and thus the increased error, does not contain the feature.

Examining the error differences globally, the biggest beneficial impact from assimilating geostationary IR sounder observations is present in the tropics, coincident with the broadest areal coverage of observations. Degradation occurs over the South Polar region where it is austral winter and near the tropical tropopause. Globally, the advantage of a ring of GEO IR sounders, consistent with the vision of the WMO (WMO 2019) is apparent. Over the tropics, the improvement obtained from the GXS-Only experiment is on the order of 1%–2%; however, if two additional GEO sounders are included, the improvement is closer to 5%, and this result extends throughout the tropical tropospheric column and over a broader range of latitudes.

Within the smaller domains, the advantage of the global ring over assimilating only GXS is less significant. In both experiments over the GXS defined domain, there is an overall error reduction that can be achieved almost entirely by the additional assimilation of GXS beyond the Control. The low tropospheric degradation in this domain is associated with the low cloud decks over cold water, west of South America. This may be related to difficulties in properly representing stratocumulus clouds in this region and differences in the

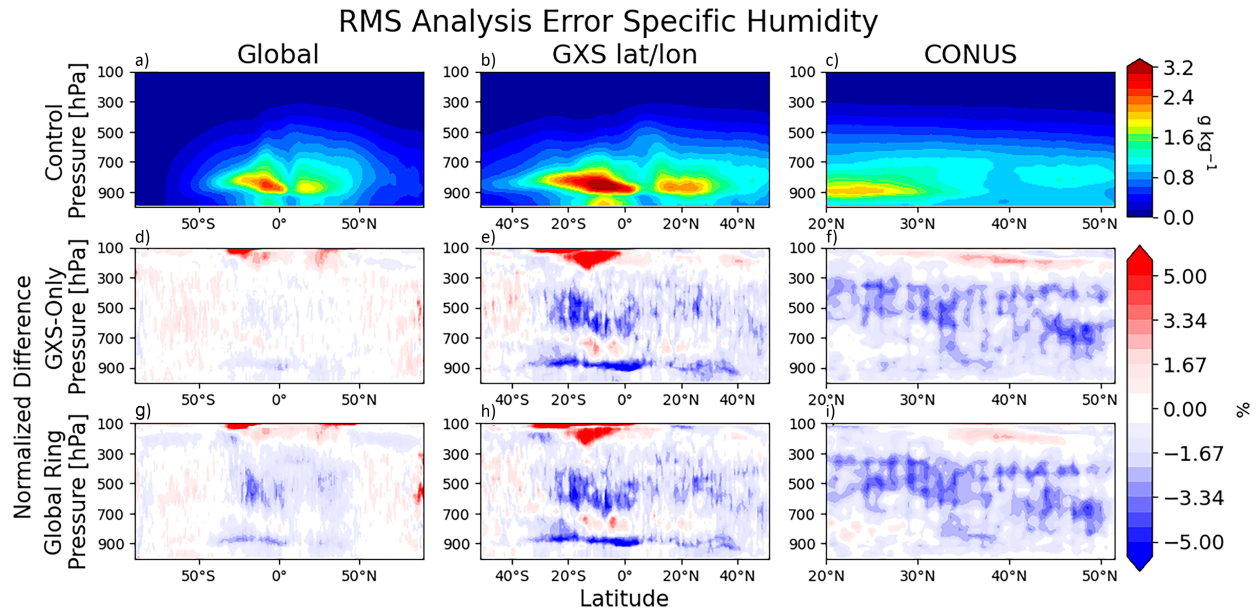


FIG. 4. As in Fig. 3, but for specific humidity (g kg^{-1}).

microphysics and boundary layer parameterizations used in the DAS and the nature run. Specifically, the assimilation of GEO IR observations results in, on average, a beneficial cooling from approximately 900 to 750 hPa. Because of the weighting functions associated with the radiance observations, this cooling is not added as a point measurement, but is instead spread vertically, resulting in the degradation aloft of 750 hPa.

The GeoXO program is particularly interested in impacts over CONUS as one of its aims is to improve weather prediction in this area. Although CONUS is heavily observed in reality and in the Control simulation, the GXS observations contribute to a general improvement in this domain beyond what is achievable with current observations. In the right panels of Fig. 3, there are only minor differences between the two perturbation experiments with much of the benefit deriving from the assimilation of GXS, though some positive benefit comes from the broader coverage of the global ring, such as between 700 and 500 hPa south of 30°N.

In addition to temperature sensitive channels, water vapor sensitive channels from the simulated geostationary IR sounders were assimilated, thus impacting the representation of specific humidity in the perturbation experiments (Fig. 4). The largest specific humidity RMSE in the Control simulation occurs where water vapor concentrations are the highest, namely, in the troposphere and more specifically in the tropics. These larger RMSE exist predominantly equatorward of 30°N/S and between 900 and 700 hPa. Similarly to the RMSE of temperature, this elevated error region is associated with low-level cloud decks off the west coast of South America as well as Africa. Given the larger fractional coverage of these regions in the GXS domain (middle panel), this error feature is larger than in the global domain and largely absent over the CONUS domain.

The normalized differences in the perturbation experiments, relative to the Control, are shown in the lower panels of Fig. 4. Over the global domain, the GXS-Only experiment shows mixed results with a relatively weak overall beneficial impact in the tropics. When comparing with the Global Ring experiment, the importance of multiple hyperspectral IR sounders is evident with a much larger and broader beneficial impact throughout the tropical troposphere. The broad coverage in the tropics of the geostationary sounders, shown in Fig. 1, contributes to this effect.

Over the smaller domains, the significance of the global ring declines and the dominant contributor to the beneficial impact is the GXS instrument, with only slight differences between the GXS-Only and Global Ring experiments. The predominant effect of assimilating geostationary IR sounders over the GXS domain is beneficial, with reduced error in the estimation of specific humidity throughout most of the column. A small region of degradation is present near the Southern Hemisphere tropical tropopause.

Similarly, over the CONUS domain in the rightmost panels, there are only small differences between the GXS-Only and the Global Ring perturbation experiments. Assimilation of GXS results in a comprehensive improvement in the tropospheric specific humidity estimation. Particularly, the improvement is largest below 300 hPa where specific humidity values are greatest.

In addition to the directly observed variables, the high temporal resolution and low data latency provides data on the winds through observations of rapidly evolving phenomena. Wind increments may be inferred through covariances between the wind and directly observed variables in the DAS, such as specific humidity (Peubey and McNally 2009), providing new information content to the DAS. Furthermore, an improved estimate of the winds contributes to improved estimates of tracer transport and their subsequent concentrations.

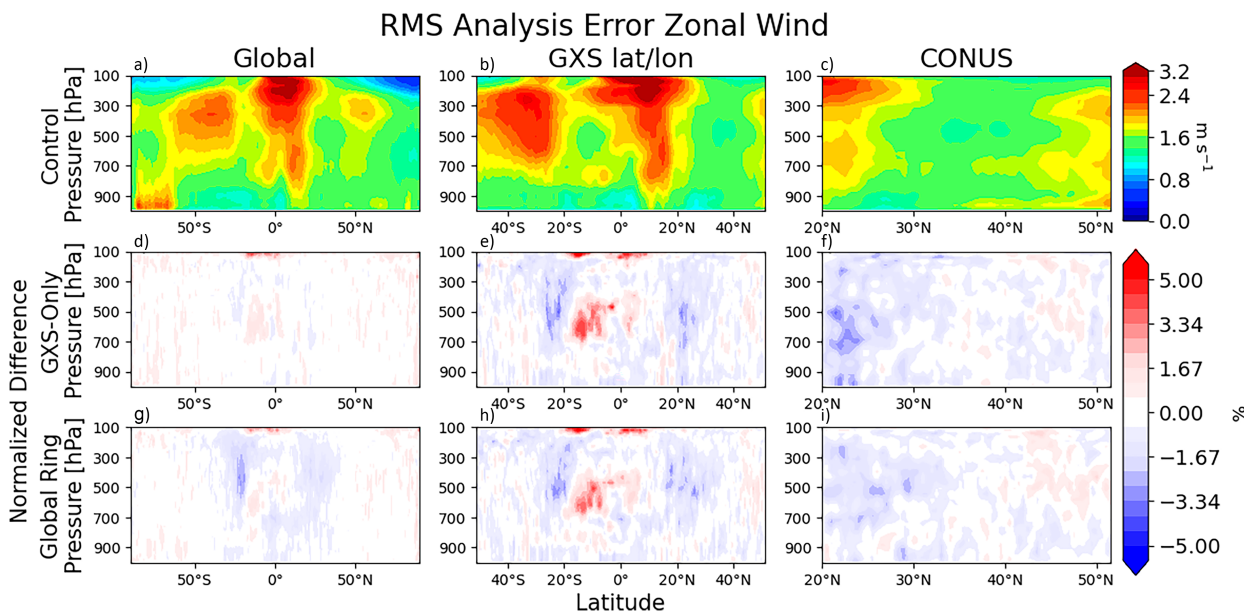


FIG. 5. As in Fig. 3, but for zonal wind (m s^{-1}).

An examination of the error patterns of the zonal and meridional winds is provided in Figs. 5 and 6, respectively. The locations of the greatest zonally averaged RMSE in the Control are consistent with the midlatitude and tropical easterly jets, most obvious in the global panel. The pattern is similar over the GXS domain with an increased magnitude of error in the Southern Hemisphere midlatitude jet due to RMSE increases in the vicinity of South America and the surrounding oceans. Within the CONUS domain, the largest magnitude error is focused aloft of 300 hPa and south of 30°N with an

additional error distributed throughout the tropospheric column north of about 50°N. The locations and magnitudes are similar between the zonal and meridional winds.

Similar to other analysis results, the global pattern of normalized difference in the perturbation experiments depends on the global coverage of geostationary IR sounders with the Global Ring experiment resulting in more coherent differences than assimilating GXS alone. Both wind components show mixed results in the global domain for the GXS-Only experiment, but a largely beneficial impact throughout the

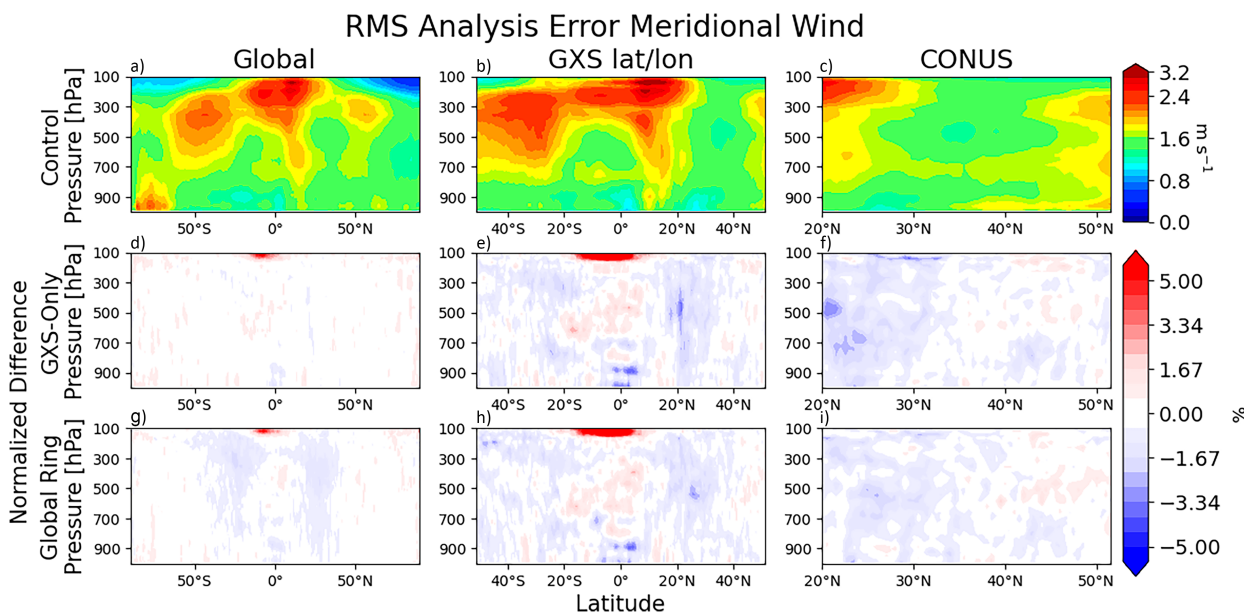


FIG. 6. As in Fig. 3, but for meridional wind (m s^{-1}).

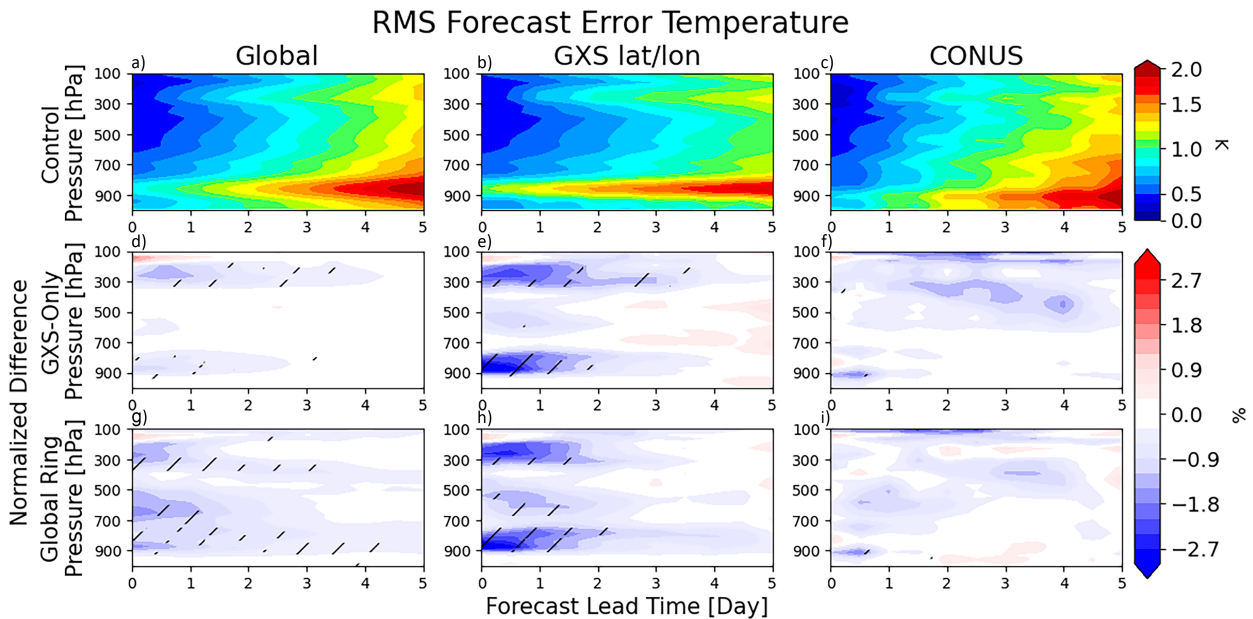


FIG. 7. Domain-averaged (a)–(c) RMSE for temperature (K) in the Control vs the nature run as a function of pressure and forecast time, (d)–(f) the normalized change in RMSE (%) relative to the Control in the GXS-Only experiment, and (g)–(i) The normalized change in RMSE (%) relative to the Control in the Global Ring experiment for the (left) global, (center) GXS-defined latitudes and longitudes, and (right) CONUS regions. Calculations are done for the 0000 UTC forecasts only. In the difference plots, blue or red indicates an improvement or degradation, respectively, by the addition of the geostationary IR radiances and hatching indicates statistical significance at the 90% level, taking into account autocorrelation.

tropical troposphere roughly equatorward of 30°N/S when the global ring is assimilated.

However, over the smaller domains where observations from GXS are the only geostationary IR sounder data assimilated, there are much smaller differences between the GXS-Only and Global Ring experiments. In the GXS domain (middle panels), the wind estimation in much of the extratropics poleward of about 20°N/S benefits from the assimilation of geostationary IR radiances, specifically from GXS. A degradation from about the equator to 10°S and between 700 and 500 hPa is associated with a degradation to the west of South America, at roughly 110°W. This effect in the tropics is not surprising given the weaker relationship between temperature and wind in this region and thus the weaker ability for the covariances to provide beneficial information about the winds. The CONUS domain (right panels) is entirely within the extratropics and the impact of geostationary IR radiances is largely beneficial, particularly at the lower latitudes of this domain.

NWP forecasts rely on analyses for initialization, so an impact on the analysis directly impacts the predictive skill of the subsequent forecast. The improvements shown above are therefore necessary for better weather forecasts.

b. Forecast

In both the Northern (20°–80°N) and Southern (80°–20°S) Hemisphere extratropics, the anomaly correlation for 500-hPa geopotential height was examined (not shown). The effect of the perturbation experiments in the Southern Hemisphere

was statistically significant, but the differences were small improvements in the short-range forecasts that did not persist through time. In the Northern Hemisphere, however, there was more of a statistically significant improvement, specifically in the short- and long-range forecasts in the Global Ring perturbation experiment extending to 7 days. This highlights the importance of global coverage from geostationary IR sounders for the improvement of global numerical weather prediction.

The effect of assimilating geostationary IR sounders on temperature forecasts is shown in Fig. 7. The top row shows the RMSE as a function of pressure and forecast time validated against the G5NR. Consistent with real forecasts, this error grows with time. The bottom two rows show the normalized differences of the GXS-Only and Global Ring perturbation experiments from the Control. These are shown for the same three domains used in the evaluation of the analysis errors: global, the latitudes and longitudes observed by the GXS instrument, and over the CONUS domain.

Prior work (e.g., Privé and Errico 2013; Cucurull and Casey 2021; Privé et al. 2022) has shown that the largest impacts generally occur during the early forecast periods and this is especially true over the tropics and the summer hemisphere. The results of Fig. 7 are consistent with this result, showing statistically significant impacts during the earliest parts of the forecasts. In the global domain, these extend to approximately 3 days in both the GXS-Only and Global Ring perturbation experiments. For GXS-Only, the beneficial impacts exist in three distinct layers near 900, 600, and 300 hPa with the upper

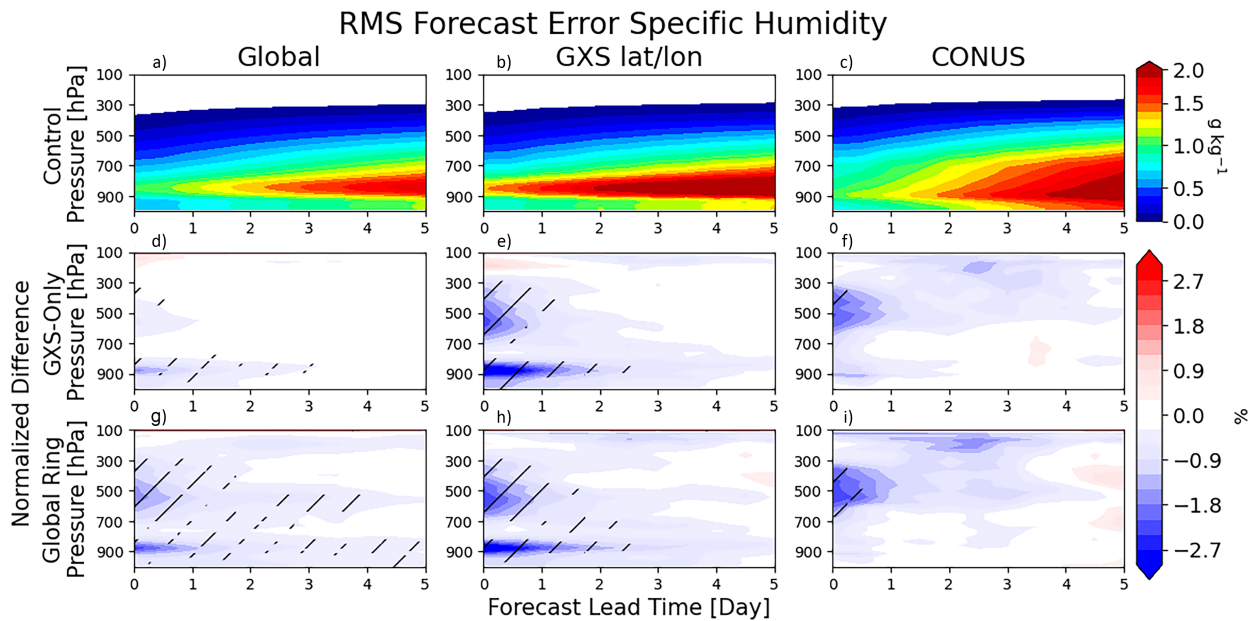


FIG. 8. As in Fig. 7, but for specific humidity (g kg^{-1}).

tropospheric impact being the largest and extending the longest. Only the lower and upper levels show statistically significant improvements. In the Global Ring experiment, the effect of broader longitudinal coverage from the additional geostationary sounders is more consistent with a larger forecast improvement throughout the troposphere and a greater statistical significance. Interestingly, the band at 600 hPa has a stronger beneficial impact in the Global Ring experiment than the other two bands, in contrast with the GXS-Only experiment.

In the middle column, the effect is highlighted over the GXS-defined domains of the Western Hemisphere. The beneficial impact is again concentrated in three bands, but with a larger intensity than in the global domain. The statistical significance in the upper troposphere extends to about three days in the GXS-Only experiment, slightly longer than in the Global Ring perturbation. The Global Ring experiment is more consistent throughout the troposphere with significance until approximately 2 days. As in the global domain, the intensity of the midtropospheric improvement at 600 hPa is larger in the Global Ring experiment than in the GXS-Only experiment.

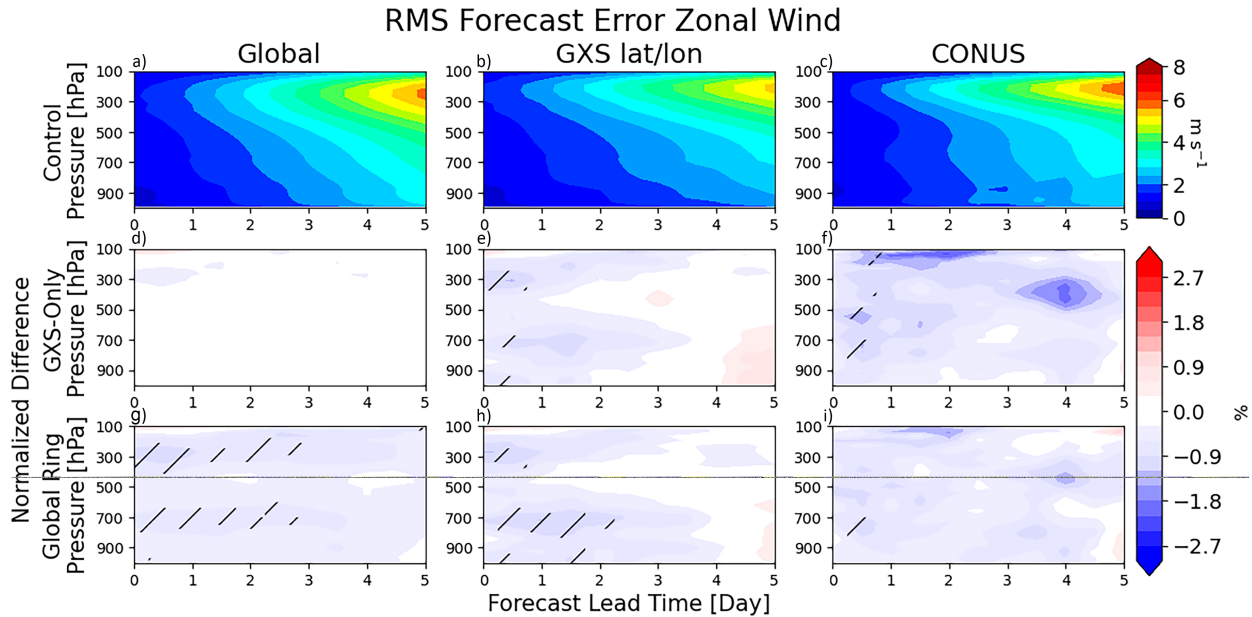
Over the CONUS domain, shown on the far right, the effect of assimilating geostationary IR sounders in either perturbation experiment is mostly positive though the impact is small and generally insignificant. The Global Ring slightly degrades the forecast in comparison with assimilating GXS only, but the effect is small and not statistically significant.

Error growth of the specific humidity forecast and the normalized difference of the two perturbation experiments relative to the Control are shown in Fig. 8. In the Control, the errors are predominantly in the lower troposphere where water vapor concentrations are highest. The largest errors are at approximately 800 hPa, growing with forecast time.

Over the global domain, the GXS-Only experiment produces a statistically significant short-term beneficial impact on humidity in the midtroposphere and an even larger beneficial impact in the lower troposphere extending to 3 days. Beyond these, there is minimal impact from assimilating the GXS instrument. By expanding the geostationary IR coverage in the Global Ring experiment, the improvement is increased with a statistically significant beneficial impact extending throughout most of the troposphere and beyond 4 days in the lower troposphere. Much of the improvement occurs in the midtroposphere from about 700 to 300 hPa with statistical significance beyond 3 days. Given the large improvement in the Global Ring experiment in the analyses used for the initialization of these forecasts, it is not surprising that the inclusion of additional GEO IR sounders produces such a beneficial result.

Zooming in on the GXS defined domain, the differences between the perturbation experiments decline with nearly identical impacts whether GXS only is assimilated or if the global ring is included. In both experiments, the beneficial impact extends throughout the troposphere, but is most significant around 900 hPa to almost 3 days and in the midtroposphere until approximately 1 day. This is somewhat shorter than in the global domain, most likely due to a smaller extratropical areal fraction. Error growth in the tropics is dominated more by fast convective processes rather than the slow baroclinic processes that dominate farther poleward. In both this and the global domain, the lower tropospheric improvement at the level of the low-level cloud decks is meaningful for reducing errors in the regions of highest uncertainty.

Differences on the CONUS domain between the perturbation experiments (the right side of Fig. 8) are also small. In both experiments, assimilating geostationary sounders results in a beneficial impact throughout the troposphere, but is only

FIG. 9. As in Fig. 7, but for zonal wind (m s^{-1}).

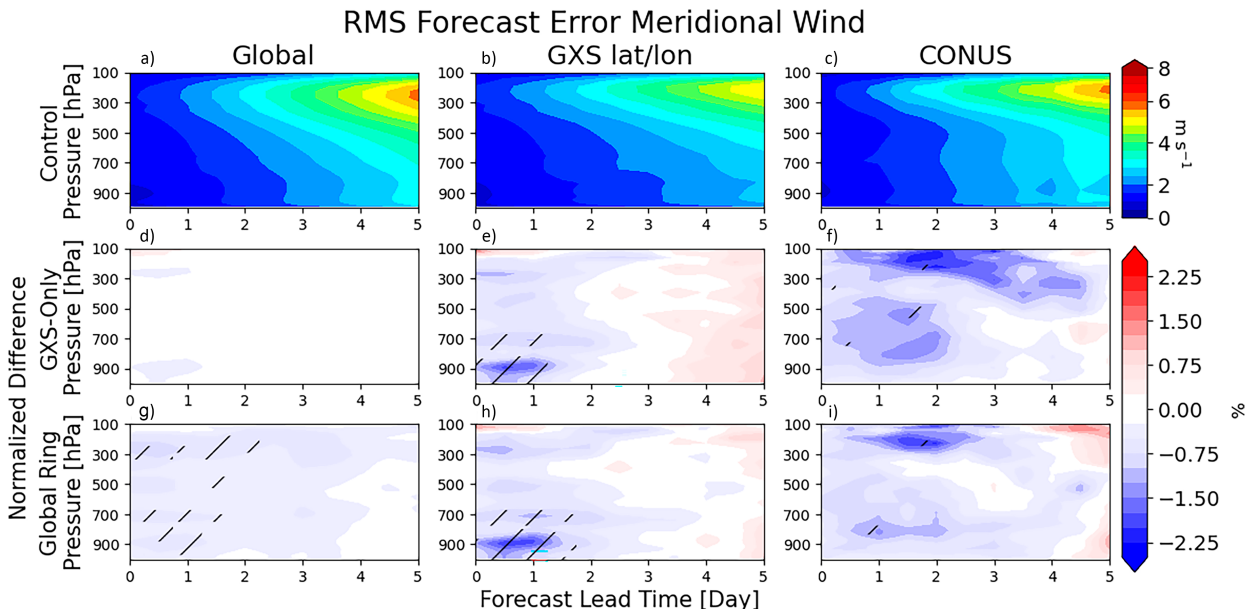
significant in the midtroposphere at ~ 500 hPa. The minimal impact of the global ring on this domain indicates that this beneficial impact is a result of assimilating GXS and may be achieved without the international coverage.

One of the main advantages of a sounder from a geostationary platform is that the high temporal resolution provides information on the winds through covariances between the wind and directly observed variables, such as specific humidity. Despite the 6-h assimilation window used, this effect, plus other improvements in the analyses used to initialize the

forward in time forecasts, impacts the prediction of wind velocity (Figs. 9 and 10).

In the Control experiment, shown in the top rows of Figs. 9 and 10, the RMSE grows with time in each domain and is largest in the upper troposphere, consistent with the height of the midlatitude and tropical easterly jets. The error magnitudes and progression with time are similar between the zonal and meridional winds.

In the global domain (left panels), the impact of the GXS-Only perturbation experiment is minimal with very small

FIG. 10. As in Fig. 7, but for meridional wind (m s^{-1}).

normalized differences relative to the Control. The global prediction of wind velocity is unaffected by assimilation of GXS observations. However, in the Global Ring perturbation experiment, the effect is more extensive. Wind improvements, relative to the Control, exist throughout the troposphere for both wind components extending for the most part out to 2 days and beyond 3 days at approximately 700 hPa for the zonal wind. This difference in predictability behavior between the GXS-Only and Global Ring experiments is consistent with the effect observed in the analysis (Figs. 5 and 6) where the longitudinal coverage of geostationary sounders was critical to improvements in global wind representation.

On the smaller, GXS-defined domain (middle panels), the effect of the global ring is less crucial. Both perturbation experiments produce a similar beneficial impact on the forecast of wind velocity throughout the troposphere, with larger intensity for the meridional wind. The zonal wind forecast improvement is significant to approximately 0.5 days from near the surface to approximately 700 hPa and at around 300 hPa, near the height of the midlatitude jets in the GXS-Only experiment. The statistical significance of the near-surface improvement extends to approximately 2 days in the Global Ring experiment. The meridional wind experiences a larger intensity improvement throughout the troposphere, especially near the surface to approximately 900 hPa. This improvement extends through the 1 day forecast and out to almost 2 days at 700 hPa in the Global Ring experiment. On this domain, there exists a small degradation, particularly for the meridional wind beyond the 4 day forecast that is statistically insignificant and shows that the positive impact from the improved initialization weakens as model error and chaotic error growth dominate the forecasts.

Over the CONUS domain (right panels), the effect of geostationary sounder assimilation in both the GXS-Only and Global Ring perturbation experiments produces significant beneficial improvements only over a small portion of the forecasts, mostly between 900 and 500 hPa and for less than 1 day for both wind components. Although generally insignificant, the overwhelming impact of geostationary sounder assimilation in both experiments is beneficial before day 4. An improvement in the upper troposphere in both components, although particularly for the meridional wind, is consistent with the height of the largest error in the Control.

c. Hurricanes

Previous tropical cyclone case studies (e.g., Atlas et al. 2015; McNoldy et al. 2017; Okamoto et al. 2020) have shown the effectiveness of OSSEs in estimating the impact of future sensors on these systems. The experiments examined here were extended into the month of September to capture several Atlantic Ocean hurricanes present in the G5NR. Five-day forecasts were generated for every analysis cycle (0000, 0600, 1200, and 1800 UTC) during September to provide more robust statistics. Three hurricanes occurred within the observational domain of GXS and were thus sampled by the instrument. AL03 traveled across the Gulf of Mexico from 7 to 11 September, making landfall along the Mississippi and

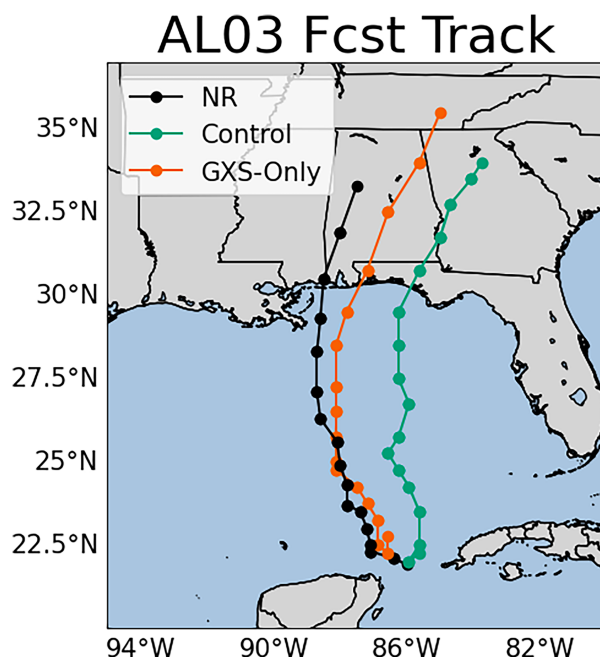


FIG. 11. The TC track from the Nature Run (black) and forecasts for AL03 initialized at 1800 UTC 7 Sep from the Control (green) and GXS-Only (orange) experiment. Dots indicate the manually tracked position every 6 h.

Alabama border (Fig. 11). AL04 was particularly long lived (from 12 to 27 September), traveling northwestward across the North Atlantic Ocean before turning northeastward well off the coast of North Carolina on 26 September. The third hurricane, AL07, was short-lived (from 29 September to 1 October) and stayed within the Gulf of Mexico, moving northerly along a nearly straight line at approximately 92°W and never made landfall.

Figure 12 examines the combined average forecast track error for the three hurricanes (AL03, AL04, and AL07) and the number of forecasts used in their calculations. The number of forecasts decreased with forecast lead time. For the three storms combined, the initial analysis (forecast lead day 0) included over 80 track estimates. When comparing the three experiments, Control, GXS-Only, and the Global Ring, it is seen that there were no statistically significant differences in the average track errors. However, there is a small improvement (on the order of 6.5% at day 5) in the Global Ring experiment relative to the Control. This predominantly resulted from improvements in the forecast track of AL04 (not shown). AL04 initially developed to the east of the GXS observational domain and is thus not observed by this instrument during its early phases. Instead, it is under the domain observed by MTG-S before traveling westward and into the GXS domain. Early forecasts, when the track is less certain, therefore rely on improvements from assimilating MTG-S. The initial 10 forecasts, while the storm is to the east of the GXS observations, do show a statistically significant forecast track improvement, relative to the Control, for forecast lead times between 2 and 4 days, highlighting the importance of

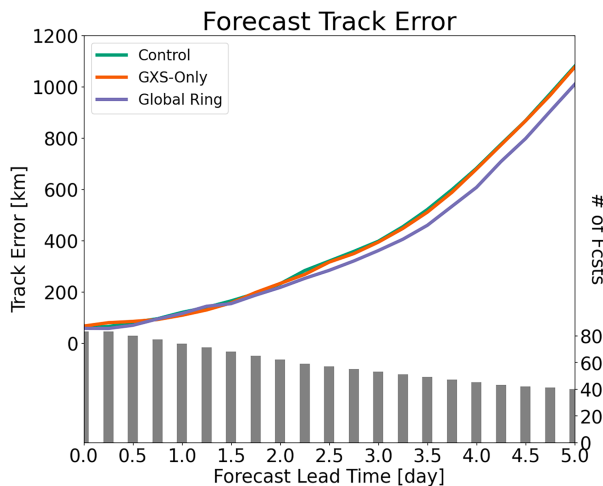


FIG. 12. Mean forecast track error (km) as a function of forecast lead time and the number of forecasts used in the computation for hurricanes AL03, AL04, and AL07 in the G5NR.

international cooperation for the improvement of this storm. Another storm, WP11 in the Northwest Pacific, occurred under the Himawari-10 observational domain. The Global Ring experiment resulted in a statistically significant improvement in average forecast track error from roughly 2 to 3 days (not shown), further highlighting the importance of international partnerships.

Focusing on a single storm, AL03, that was observed by GXS for the duration of its lifespan, the average forecast track error is shown in Fig. 13. While the sample size is expectedly smaller than for the combination of the three storms in Fig. 12, there is still a fairly robust sample size with 16 track estimates at zero lead time. The GXS-Only experiment had a track error that was consistently smaller than the error in the Control. This smaller track error, due to the assimilation of the GXS instrument, exceeds 90% significance with forecast lead times between 18 and 60 h. The later improvements are relevant to hurricane evacuations, which require forecasts on the time scales of 2–4 days (Lauer et al. 2021).

The predictability of AL03 was particularly low in its early stages when it was at its weakest. Focusing on the earliest forecast time for AL03 (1800 UTC 7 September), Fig. 11 shows track forecasts from the Control and GXS-Only experiment. From the beginning of the forecast, GXS-Only better matches the actual track as the storm moves northwestward through the Gulf of Mexico while the Control forecast track moves more directly northward. This was associated with a weak high pressure system to the northeast that was modified by the assimilation of GXS radiances to better steer the hurricane in the right direction. Around 10 September the GXS-Only track begins to diverge from the Nature Run track slightly but is still much closer to the truth than was the Control. At landfall, on 11 September, the Nature Run hurricane strikes the Mississippi and Alabama border while the GXS-Only hurricane makes landfall just to the east of Mobile Bay. The forecast from the Control lands much farther to the east,

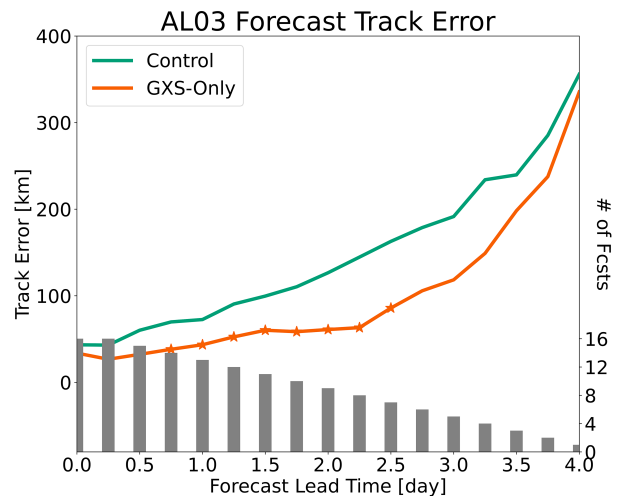


FIG. 13. Mean forecast track error (km) as a function of forecast lead time and the number of forecasts used in the computation for hurricane AL03 in the G5NR. Stars indicate significance at the 90% level.

near Panama City, Florida. At landfall, the Control has a track error of approximately 250 km, nearly 150 km more than in the GXS-only experiment.

d. FSOI

The impact of geostationary hyperspectral IR radiances can be characterized using the FSOI metric described by Langland and Baker (e.g., 2004), Zhu and Gelaro (e.g., 2008), and Gelaro and Zhu (e.g., 2009). Although not a strict ranking of instrument impact, this metric quantifies how individual observations impact the 24-h forecast moist energy error norm (Ehrendorfer et al. 1999; Holdaway et al. 2014). It may be used to create generalized groupings of high-impact instrument types for an approximate understanding of their significance in the reduction of forecast error within a NWP system. Extensive effort has been made to validate this OSSE framework to ensure a statistical resemblance to the semioperational system run by the GMAO, including for the FSOI metric and assimilated hyperspectral IR observations (Errico et al. 2013; Privé et al. 2021; El Akkraoui et al. 2023; Privé et al. 2023; McGrath-Spangler et al. 2022).

The global 24-h satellite radiance FSOI error impact is shown in Fig. 14 for the Global Ring experiment. Similar results were found for the GXS-Only experiment. This was computed using only the 0000 UTC forecasts since the forecast initialization time is less important when examining a globally computed metric. It is apparent that polar-orbiting instruments perform better than those in a geostationary orbit. This is due to the differing spatial coverage, as measured globally, of the two types of orbit. Polar orbiters sample the full domain and the disadvantage of the low temporal resolution of a given region over the diurnal cycle is not keenly perceived by the system. Conversely, instruments in a geostationary orbit provide limited information content to the global system outside their observational domain and the high

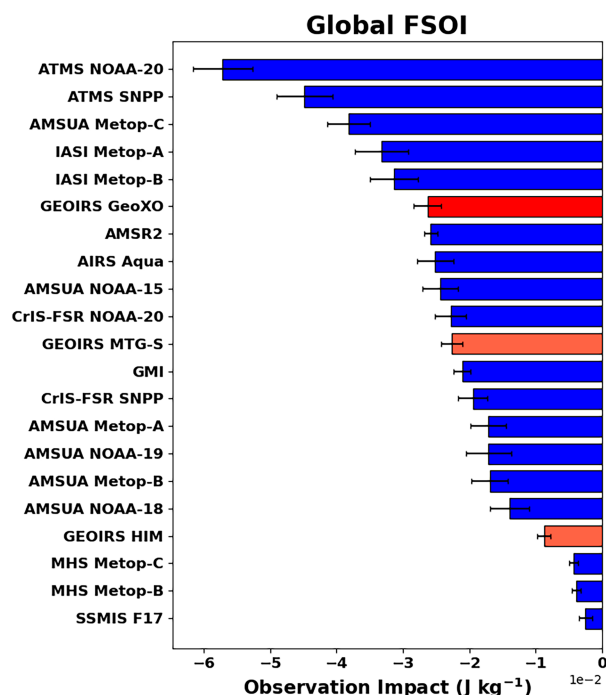


FIG. 14. FSOI per analysis as a function of satellite radiance instrument calculated globally for the 0000 UTC analyses, with error bars computed at the 90% significance level. The impact computed from GXs is highlighted in red, and the impact from the other geostationary sounders is highlighted in pink.

temporal resolution does not eliminate observational deficiencies in remote locations.

Given these limitations, GXs perform well in the global FSOI metric. Its position in the upper third most impactful satellite radiances conveys its importance in error reduction consistent with what was shown in section 5b. The impact of MTG-IRS and Himawari-10 GHMS are lower in the Global FSOI metric and this is potentially due to fewer observations being assimilated (Fig. 2) and the fast error growth associated with the convective nature of the west Pacific. Overall, the number of MTG-IRS observations assimilated is approximately 90% of the number of GXs observations. The number of assimilated GHMS observations is approximately 78% of the number of assimilated GXs observations (not shown). Radiance channels sensitive to emissivity and the surface are preferentially discarded by the quality-control algorithm over deserts, which encompass a larger fractional area of the observational domains of MTG-IRS and GHMS resulting in fewer assimilated observations from these instruments. Additionally, large fractions of high cloud cover over the western Pacific Ocean obscure much of the troposphere, further reducing assimilated observation counts from GHMS. Fast error growth limits the impact of initial condition improvements as these improvements are quickly overwhelmed by chaotic error growth associated with quick convective processes, thereby restricting the potential to improve 24-h forecast error. These effects may explain some of the relative importance of

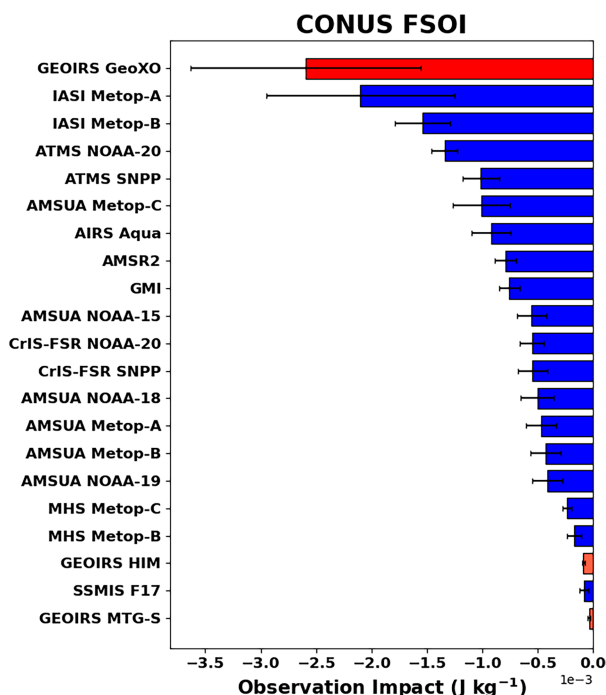


FIG. 15. FSOI per analysis as a function of satellite radiance instrument calculated over CONUS for the 0000, 0600, 1200, and 1800 UTC analyses, with error bars computed at the 90% significance level. The impact computed from GXs is highlighted in red, and the impact from the other geostationary sounders is highlighted in pink.

these instruments in error reduction as measured by the FSOI metric.

On the scale of CONUS, the FSOI result is very different from the global metric. Figure 15 shows the FSOI computed for the four synoptic times (0000, 0600, 1200, and 1800 UTC) over the CONUS domain (130°–60°W longitude and between 20° and 52°N latitude). Over the more limited spatial domain and across the full diurnal cycle, geostationary instruments observing the relevant spatiotemporal region have a clear advantage, relative to the polar orbiters, on impacting the 24-h forecast error. Polar-orbiting instruments may only observe over CONUS twice per day and cannot emulate the temporal resolution of a geostationary instrument that provides nearly continuous atmospheric sounding data (Wang et al. 2021). This critical temporal information allows a strong observational impact from the GXs instrument in reducing the moist energy error norm. Over CONUS, satellite radiances from MTG-IRS and Himawari-10 GHMS have minimal impact on energy error norm reduction over a 24-h forecast since none of their observations directly observe the region of interest (Fig. 2); however, the upstream location of Himawari-10 GHMS to the CONUS domain may provide a slight advantage over MTG-IRS in this metric.

6. Summary and conclusions

This study examined potential impacts from geostationary IR sounders from a global NWP perspective using NASA's

GMAO OSSE framework. The implied caveats and limitations of a fully simulated environment apply. This was performed with an emphasis on the NOAA/NASA proposed GeoXO Sounder both as a single IR sounder on a geostationary platform and as part of a global ring of such instruments. Specifications for the IRS instrument on the European MTG satellite were the basis for the simulated radiances. The DAS used a hybrid 4D-EnVar assimilation scheme with assumed hourly observation binning that is coarser than the proposed temporal resolution of GXS. Current DA techniques use 6-h thinning boxes that do not make optimal use of the GeoXO observations. Future developments in DA may allow better use of these observations to fully capture the high temporal frequency information.

The launch of GXS and other geostationary IR sounders has the ability to provide new, valuable information content to NWP systems through the nearly continuous vertical profiling they provide of atmospheric phenomena and processes. Current polar-orbiting IR sounders leave a knowledge gap that would be addressed by a geostationary global ring of these instruments, as identified by the WMO (2019). Additional benefits, beyond NWP, have also been identified (Lauer et al. 2021).

Four different metrics were used to assess the impact of assimilating GXS alone and as part of a global ring of such instruments. Overall, widespread improvements in the analyses occurred globally for temperature, specific humidity, and zonal and meridional wind. The wind improvements largely resulted from improved wind increments inferred from covariances of the wind with the high-temporal-resolution temperature and specific humidity observations in the DAS. The primary error reductions occurred in the tropics where the broadest span of observations exist from a geostationary platform. Globally, international contributions from MTG-IRS and Himawari-10 GHMS led to greater improvements than from assimilating GXS alone, reflective of the increased observational coverage in this domain. Specifically, the error reduction equatorward of 30° was stronger in the Global Ring experiment for all four of the evaluated thermodynamic variables. The low tropospheric degradation at about 700 hPa is associated with low cloud decks off the west coast of South America, indicating the importance of improving the handling of clouds observed by IR sensors in data assimilation systems. Regional impacts on the GXS specified and CONUS domains were primarily from the assimilation of GXS with minimal differences from the addition of the global ring.

Since the analyses were used for the initialization of the subsequent forecasts, the analysis improvements from GEO IR assimilation extended to the forecasts. Similar to the analyses, the GXS domain forecast improvements largely resulted from assimilation of GXS radiances with minimal additional improvements from the inclusion of the global ring. On the GXS specified domain, statistically significant improvements persisted throughout the tropospheric column, on the order of 2–3 days. Globally, the degree of improvements in the forecast depended more heavily on the global ring. In the GXS-Only experiment, improvements were modest and significant improvements only extended to approximately 2 days for

temperature and specific humidity. For the zonal and meridional winds, the GXS-Only experiment produced minimal improvements with only a small region of statistically significant benefit in the meridional wind at about 900 hPa that only persisted for 24 h. However, the Global Ring experiment produced much more robust improvements that extended closer to 3–4 days for temperature and specific humidity, most likely dominated by improvements in the midlatitudes. Likewise, the improvements in the wind were much more substantial in the Global Ring experiment with statistically significant improvements extending 2–3 days.

This study examined the impact of geostationary IR sounder assimilation on hurricanes. Given the constraints on the number of appropriate hurricanes available for study in any Nature Run (Atlas et al. 2015; Posselt et al. 2022), more robust statistics will be necessary once real data become available. The high temporal resolution of sounding observations available from a geostationary platform was shown to have the potential to improve hurricane forecast track errors. Averaged over 3 Atlantic hurricanes, the Global Ring experiment was able to improve the 5-day forecast by about 6.5% although this was not statistically significant. This improvement relied on observations from the European MTG-IRS instrument during the early phases of a hurricane that formed in the middle of the North Atlantic. For a Gulf of Mexico hurricane, the GXS-Only experiment was able to reduce forecast track error significantly on the time scales necessary for hurricane evacuations. For the initial forecast of this storm, the track error at landfall was nearly 150 km smaller than in the Control.

Last, the 24-h moist energy error norm reduction was examined using the FSOI metric. Globally, satellite radiance assimilation shows that the polar orbiters, which observe the full global domain, outperform the regionally focused instruments on board geostationary platforms. However, this metric, when evaluated with the higher temporal frequency and targeting the CONUS domain, shows the potential of hyperspectral IR instruments on a GEO platform. GXS, which samples CONUS with a high temporal frequency, has the largest impact on the 24-h forecast error reduction of all the radiance types.

These results must be considered in the context of several limitations. One is that explicit errors have not been added to the assimilated GEO IR observations. GXS is still in development and as such the error magnitude is yet unknown and uncertainty exists in its estimation. The presented results are therefore an upper limitation on the utility of the GXS and other geostationary IR sounders simulated in these experiments; however, the lack of optimal assimilation scheme does mitigate some of this potential impact. Additionally, the channel selection for use in NWP has not yet been determined and may affect future results. The number of channels assimilated here is relatively small in comparison with polar-orbiting IR sounders, potentially further limiting the impact of GEO sounders. The assimilated channels in this study are assumed uncorrelated although the actual instrument is likely to suffer error correlation and this source of error should be addressed when real data become available.

This investigation differs from the study of McGrath-Spangler et al. (2022) in several important ways. Perhaps most consequential, the DAS framework and observing system have been updated as described in more detail by Privé et al. (2023). As part of the observing system update, the assimilated CrIS data transitioned from nominal spectral resolution (NSR) to full spectral resolution (FSR). This study, focused on the impact of international collaboration between JMA, EUMETSAT, and NOAA/NASA, has extended the analysis to include the month of September and the associated tropical cyclones present in the Nature Run during that month. Additionally, stratospheric temperature channels that are outside the proposed range of GXS that were assimilated in the previous study have been excluded. The most pronounced difference from the previous study is better results in the Southern Hemisphere midlatitudes due to improvements in the data assimilation system.

One important goal of proposed weather instruments is to improve weather forecast prediction and the representation of atmospheric phenomena in NWP models. The capability of the proposed NOAA/NASA GXS instrument both as a single sounder on a geostationary platform and as part of an internationally supported global ring of such instruments was assessed in the context of this goal. Regionally over much of the Western Hemisphere directly observed by GXS and over the smaller CONUS region, assimilation of GXS radiances is the predominant geostationary instrument responsible for analysis improvements and forecast error reduction. In particular, the GXS instrument has the largest impact on moist energy error norm reduction as measured by the FSOI over CONUS. Globally, international partnerships on geostationary platforms play a more important role in NWP improvements. Progress toward all-sky IR assimilation offers the potential for even greater improvements, as has been shown by studies evaluating the impact of cloud-cleared radiances (e.g., Wang et al. 2015; Reale et al. 2018; Wang et al. 2019; McGrath-Spangler et al. 2021; Ganeshan et al. 2022). As real data become available from international partners and is assimilated in data assimilation systems, understanding of the future impacts of GXS will improve.

Acknowledgments. The authors gratefully acknowledge allowances on the NASA High-End Computing resources and Ron Errico for developing the baseline OSSE system. Funding was provided by the NOAA and NASA GeoXO Project. The software for simulating GPSRO observations was provided by the Radio Occultation Processing Package (ROPP) of the Radio Occultation Meteorology (ROM) Satellite Applications Facility (SAF) of EUMETSAT, with the assistance of Sean Healy at ECMWF. Resources supporting this work were provided by the NASA High-End Computing (HEC) Program through the NASA Center for Climate Simulation (NCCS) at Goddard Space Flight Center. The authors also thank three anonymous reviewers, whose comments provided valuable feedback to improving this paper.

Data availability statement. Documentation and methods used to support this study are available from the lead author

at NASA GMAO because the dataset on which this paper is based is too large to be retained or made publicly available with available resources. The G5NR is available for download from an online portal (https://gmao.gsfc.nasa.gov/global_mesoscale/7km-G5NR). The codes used to generate simulated observations are available on GitHub (<https://github.com/GEOS-ESM/GOWASP>).

REFERENCES

- Arnold, C. P., Jr., and C. H. Dey, 1986: Observing-systems simulation experiments: Past, present, and future. *Bull. Amer. Meteor. Soc.*, **67**, 687–695, [https://doi.org/10.1175/1520-0477\(1986\)067<0687:OSSEPP>2.0.CO;2](https://doi.org/10.1175/1520-0477(1986)067<0687:OSSEPP>2.0.CO;2).
- Atlas, R., E. Kalnay, and M. Halem, 1985: Impact of satellite temperature sounding and wind data on numerical weather prediction. *Opt. Eng.*, **24**, 242341, <https://doi.org/10.1117/12.7973481>.
- , L. Bucci, B. Annane, R. Hoffman, and S. Murillo, 2015: Observing system simulation experiments to assess the potential impact of new observing systems on hurricane forecasting. *Mar. Technol. Soc. J.*, **49**, 140–148, <https://doi.org/10.4031/MTSJ.49.6.3>.
- Bacmeister, J. T., M. J. Suarez, and F. R. Robertson, 2006: Rain reevaporation, boundary layer–convection interactions, and Pacific rainfall patterns in an AGCM. *J. Atmos. Sci.*, **63**, 3383–3403, <https://doi.org/10.1175/JAS3791.1>.
- Barahona, D., A. Molod, J. Bacmeister, A. Nenes, A. Gettelman, H. Morrison, V. Phillips, and A. Eichmann, 2014: Development of two-moment cloud microphysics for liquid and ice within the NASA Goddard Earth Observing System Model (GEOS-5). *Geosci. Model Dev.*, **7**, 1733–1766, <https://doi.org/10.5194/gmd-7-1733-2014>.
- Bessho, K., H. Owada, K. Okamoto, and T. Fujita, 2021: Himawari-8/9 follow-on satellite program and impacts of potential usage of hyperspectral IR sounder. *IEEE Int. Geoscience and Remote Sensing Symp.*, Brussels, Belgium, IEEE, 1507–1510, <https://doi.org/10.1109/IGARSS47720.2021.9553888>.
- Chahine, M. T., and Coauthors, 2006: AIRS: Improving weather forecasting and providing new data on greenhouse gases. *Bull. Amer. Meteor. Soc.*, **87**, 911–926, <https://doi.org/10.1175/BAMS-87-7-911>.
- Chen, Y., F. Weng, Y. Han, and Q. Liu, 2008: Validation of the community radiative transfer model by using CloudSat data. *J. Geophys. Res.*, **113**, D00A03, <https://doi.org/10.1029/2007JD009561>.
- Coopmann, O., N. Fourrié, and V. Guidard, 2022: Analysis of MTG-IRS observations and general channel selection for numerical weather prediction models. *Quart. J. Roy. Meteor. Soc.*, **148**, 1864–1885, <https://doi.org/10.1002/qj.4282>.
- , —, P. Chambon, J. Vidot, P. Brousseau, M. Martet, and C. Birman, 2023: Preparing the assimilation of the future MTG-IRS sounder into the mesoscale numerical weather prediction AROME model. *Quart. J. Roy. Meteor. Soc.*, **149**, 3110–3134, <https://doi.org/10.1002/qj.4548>.
- Cucurull, L., and S. P. F. Casey, 2021: Improved impacts in observing system simulation experiments of radio occultation observations as a result of model and data assimilation changes. *Mon. Wea. Rev.*, **149**, 207–220, <https://doi.org/10.1175/MWR-D-20-0174.1>.
- Ding, S., P. Yang, F. Weng, Q. Liu, Y. Han, P. van Delst, J. Li, and B. Baum, 2011: Validation of the Community Radiative

- Transfer Model. *J. Quant. Spectrosc. Radiat. Transfer*, **112**, 1050–1064, <https://doi.org/10.1016/j.jqsrt.2010.11.009>.
- Ehrendorfer, M., R. M. Errico, and K. D. Raeder, 1999: Singular-vector perturbation growth in a primitive equation model with moist physics. *J. Atmos. Sci.*, **56**, 1627–1648, [https://doi.org/10.1175/1520-0469\(1999\)056<1627:SVPGIA>2.0.CO;2](https://doi.org/10.1175/1520-0469(1999)056<1627:SVPGIA>2.0.CO;2).
- El Akkraoui, A., N. C. Privé, R. M. Errico, and R. Todling, 2023: The GMAO hybrid 4D-EnVar observing system simulation experiment framework. *Mon. Wea. Rev.*, **151**, 1717–1734, <https://doi.org/10.1175/MWR-D-22-0254.1>.
- Errico, R. M., and N. C. Privé, 2018: Some general and fundamental requirements for designing observing system simulation experiments (OSSEs). WMO Tech. Rep. WWRP 2018-8, 24 pp., <https://ntrs.nasa.gov/api/citations/20190025338/downloads/20190025338.pdf>.
- , R. Yang, N. C. Privé, K.-S. Tai, R. Todling, M. E. Sienkiewicz, and J. Guo, 2013: Development and validation of observing-system simulation experiments at NASA's Global Modeling and Assimilation Office. *Quart. J. Roy. Meteor. Soc.*, **139**, 1162–1178, <https://doi.org/10.1002/qj.2027>.
- , and Coauthors, 2017: Description of the GMAO OSSE for weather analysis software package: Version 3. NASA Tech. Rep. NASA/TM-2017-104606/Vol. 48, 156 pp., <https://gmao.gsfc.nasa.gov/pubs/docs/Errico987.pdf>.
- Eyre, J. R., and W. P. Menzel, 1989: Retrieval of cloud parameters from satellite sounder data: A simulation study. *J. Appl. Meteor.*, **28**, 267–275, [https://doi.org/10.1175/1520-0450\(1989\)028%3C0267:ROCPFS%3E2.0.CO;2](https://doi.org/10.1175/1520-0450(1989)028%3C0267:ROCPFS%3E2.0.CO;2).
- Ganeshan, M., O. Reale, E. McGrath-Spangler, and N. Boukachaba, 2022: Impact of assimilating adaptively thinned AIRS cloud-cleared radiances on the analysis of polar lows and Mediterranean Sea tropical-like cyclone in a global modeling and data assimilation framework. *Wea. Forecasting*, **37**, 1117–1134, <https://doi.org/10.1175/WAF-D-21-0068.1>.
- Gelaro, R., and Y. Zhu, 2009: Examination of observation impacts derived from observing system experiments (OSEs) and adjoint models. *Tellus*, **61A**, 179–193, <https://doi.org/10.1111/j.1600-0870.2008.00388.x>.
- , and Coauthors, 2015: Evaluation of the 7-km GEOS-5 nature run. NASA Tech. Rep. NASA/TM-2014-104606/Vol. 36, 305 pp., <https://gmao.gsfc.nasa.gov/pubs/docs/Gelaro736.pdf>.
- Guo, Q., and Coauthors, 2021: Spectrum calibration of the first hyperspectral infrared measurements from a geostationary platform: Method and preliminary assessment. *Quart. J. Roy. Meteor. Soc.*, **147**, 1562–1583, <https://doi.org/10.1002/qj.3981>.
- Han, Y., P. van Delst, Q. Liu, F. Weng, B. Yan, R. Treadon, and J. Derber, 2006: Community Radiative Transfer Model (CRTM): Version 1. NOAA Tech. Rep. NESDIS 122, 33 pp., <https://repository.library.noaa.gov/view/noaa/1157>.
- Hoffman, R. N., and R. Atlas, 2016: Future observing system simulation experiments. *Bull. Amer. Meteor. Soc.*, **97**, 1601–1616, <https://doi.org/10.1175/BAMS-D-15-00200.1>.
- Holdaway, D., R. Errico, R. Gelaro, and J. G. Kim, 2014: Inclusion of linearized moist physics in NASA's Goddard Earth Observing System data assimilation tools. *Mon. Wea. Rev.*, **142**, 414–433, <https://doi.org/10.1175/MWR-D-13-00193.1>.
- Holmlund, K., and Coauthors, 2021: Meteosat Third Generation (MTG): Continuation and innovation of observations from geostationary orbit. *Bull. Amer. Meteor. Soc.*, **102**, E990–E1015, <https://doi.org/10.1175/BAMS-D-19-0304.1>.
- Ingleby, B., and Coauthors, 2021: The impact of COVID-19 on weather forecasts: A balanced view. *Geophys. Res. Lett.*, **48**, e2020GL090699, <https://doi.org/10.1029/2020GL090699>.
- Iturbide-Sanchez, F., and Coauthors, 2022: Exploration of a future NOAA infrared sounder in geostationary Earth orbit. *IEEE J. Sel. Top. Appl. Earth Obs. Remote Sens.*, **15**, 1543–1561, <https://doi.org/10.1109/JSTARS.2022.3142069>.
- Johnson, B. T., C. Dang, P. Stegmann, Q. Liu, I. Moradi, and T. Auligne, 2023: The Community Radiative Transfer Model (CRTM): Community-focused collaborative model development accelerating research to operations. *Bull. Amer. Meteor. Soc.*, **104**, E1817–E1830, <https://doi.org/10.1175/BAMS-D-22-0015.1>.
- Jones, T. A., S. Koch, and Z. Li, 2017: Assimilating synthetic hyperspectral sounder temperature and humidity retrievals to improve severe weather forecasts. *Atmos. Res.*, **186**, 9–25, <https://doi.org/10.1016/j.atmosres.2016.11.004>.
- Kleist, D. T., D. F. Parrish, J. C. Derber, R. Treadon, W.-S. Wu, and S. Lord, 2009: Introduction of the GSI into the NCEP Global Data Assimilation System. *Wea. Forecasting*, **24**, 1691–1705, <https://doi.org/10.1175/2009WAF2222201.1>.
- Langland, R. H., and N. L. Baker, 2004: Estimation of observation impact using the NRL atmospheric variational data assimilation adjoint system. *Tellus*, **56A**, 189–201, <https://doi.org/10.3402/tellusa.v56i3.14413>.
- Lauer, C., J. Conran, and J. Adkins, 2021: Estimating the societal benefits of satellite instruments: Application to a break-even analysis of the GeoXO hyperspectral IR sounder. *Front. Environ. Sci.*, **9**, 749044, <https://doi.org/10.3389/fenvs.2021.749044>.
- Li, J., W. P. Menzel, T. J. Schmit, and J. Schmetz, 2022: Applications of geostationary hyperspectral infrared sounder observations: Progress, challenges, and future perspectives. *Bull. Amer. Meteor. Soc.*, **103**, E2733–E2755, <https://doi.org/10.1175/BAMS-D-21-0328.1>.
- Li, Z., and Coauthors, 2018: Value-added impact of geostationary hyperspectral infrared sounders on local severe storm forecasts—Via a quick regional OSSE. *Adv. Atmos. Sci.*, **35**, 1217–1230, <https://doi.org/10.1007/s00376-018-8036-3>.
- Lin, S.-J., 2004: A “vertically Lagrangian” finite-volume dynamical core for global models. *Mon. Wea. Rev.*, **132**, 2293–2307, [https://doi.org/10.1175/1520-0493\(2004\)132<2293:AVLFDC>2.0.CO;2](https://doi.org/10.1175/1520-0493(2004)132<2293:AVLFDC>2.0.CO;2).
- McCarty, W., G. Jedlovec, and T. L. Miller, 2009: Impact of the assimilation of Atmospheric Infrared Sounder radiance measurements on short-term weather forecasts. *J. Geophys. Res.*, **114**, D18122, <https://doi.org/10.1029/2008JD011626>.
- , D. Carvalho, I. Moradi, and N. C. Privé, 2021: Observing system simulation experiments investigating atmospheric motion vectors and radiances from a constellation of 4–5- μm infrared sounders. *J. Atmos. Oceanic Technol.*, **38**, 331–347, <https://doi.org/10.1175/JTECH-D-20-0109.1>.
- McGrath-Spangler, E. L., M. Ganeshan, O. Reale, N. Boukachaba, W. McCarty, and R. Gelaro, 2021: Sensitivity of low-tropospheric Arctic temperatures to assimilation of AIRS cloud-cleared radiances: Impact on midlatitude waves. *Quart. J. Roy. Meteor. Soc.*, **147**, 4032–4047, <https://doi.org/10.1002/qj.4166>.
- , W. McCarty, N. C. Privé, I. Moradi, B. M. Karpowicz, and J. McCorkel, 2022: Using OSSEs to evaluate the impacts of geostationary infrared sounders. *J. Atmos. Oceanic Technol.*, **39**, 1903–1918, <https://doi.org/10.1175/JTECH-D-22-0033.1>.
- McNally, A. P., P. D. Watts, J. A. Smith, R. Engelen, G. A. Kelly, J. N. Thépaut, and M. Matricardi, 2006: The assimilation of AIRS radiance data at ECMWF. *Quart. J. Roy. Meteor. Soc.*, **132**, 935–957, <https://doi.org/10.1256/qj.04.171>.
- McNoldy, B., B. Annane, S. Majumdar, J. Delgado, L. Bucci, and R. Atlas, 2017: Impact of assimilating CYGNSS data on tropical cyclone analyses and forecasts in a regional OSSE framework.

- Mar. Technol. Soc. J.*, **51**, 7–15, <https://doi.org/10.4031/MTSJ.51.1.1>.
- Molod, A., L. Takacs, M. Suarez, and J. Bacmeister, 2015: Development of the GEOS-5 atmospheric general circulation model: Evolution from MERRA to MERRA2. *Geosci. Model Dev.*, **8**, 1339–1356, <https://doi.org/10.5194/gmd-8-1339-2015>.
- Niu, Z., L. Zhang, Y. Han, P. Dong, and W. Huang, 2023: Performances between the FY-4A/GIIRS and FY-4B/GIIRS long-wave infrared (LWIR) channels under clear-sky and all-sky conditions. *Quart. J. Roy. Meteor. Soc.*, **149**, 1612–1628, <https://doi.org/10.1002/qj.4473>.
- Noh, Y.-C., A. H. N. Lim, H.-L. Huang, and M. D. Goldberg, 2020: Global forecast impact of low data latency infrared and microwave sounders observations from polar orbiting satellites. *Remote Sens.*, **12**, 2193, <https://doi.org/10.3390/rs12142193>.
- Okamoto, K., and Coauthors, 2020: Assessment of the potential impact of a hyperspectral infrared sounder on the Himawari follow-on geostationary satellite. *SOLA*, **16**, 162–168, <https://doi.org/10.2151/sola.2020-028>.
- Pagano, T. S., M. T. Chahine, and E. J. Fetzer, 2010: The Atmospheric Infrared Sounder (AIRS) on the NASA Aqua spacecraft: A general remote sensing tool for understanding atmospheric structure, dynamics, and composition. *Proc. SPIE*, **7827**, 78270B, <https://doi.org/10.1117/12.865335>.
- Pearlman, A., M. Cook, B. Efremova, F. Padula, L. Lamsal, J. McCorkel, and J. Joiner, 2022: Polarization performance simulation for the GeoXO atmospheric composition instrument: NO₂ retrieval impacts. *Atmos. Meas. Tech.*, **15**, 4489–4501, <https://doi.org/10.5194/amt-15-4489-2022>.
- Peubey, C., and A. P. McNally, 2009: Characterization of the impact of geostationary clear-sky radiances on wind analyses in a 4D-Var context. *Quart. J. Roy. Meteor. Soc.*, **135**, 1863–1876, <https://doi.org/10.1002/qj.500>.
- Posselt, D. J., L. Wu, M. Schreier, J. Roman, M. Minamide, and B. Lambigtsen, 2022: Assessing the forecast impact of a geostationary microwave sounder using regional and global OSSEs. *Mon. Wea. Rev.*, **150**, 625–645, <https://doi.org/10.1175/MWR-D-21-0192.1>.
- Privé, N. C., and R. M. Errico, 2013: The role of model and initial condition error in numerical weather forecasting investigated with an observing system simulation experiment. *Tellus*, **65A**, 21740, <https://doi.org/10.3402/tellusa.v65i0.21740>.
- , —, and K.-S. Tai, 2014: The impact of increased frequency of rawinsonde observations on forecast skill investigated with an observing system simulation experiment. *Mon. Wea. Rev.*, **142**, 1823–1834, <https://doi.org/10.1175/MWR-D-13-00237.1>.
- , —, R. Todling, and A. El Akkraoui, 2021: Evaluation of adjoint-based observation impacts as a function of forecast length using an observing system simulation experiment. *Quart. J. Roy. Meteor. Soc.*, **147**, 121–138, <https://doi.org/10.1002/qj.3909>.
- , —, and A. El Akkraoui, 2022: Investigation of the potential saturation of information from Global Navigation Satellite System radio occultation observations with an observing system simulation experiment. *Mon. Wea. Rev.*, **150**, 1293–1316, <https://doi.org/10.1175/MWR-D-21-0230.1>.
- , E. L. McGrath-Spangler, D. Carvalho, B. Karpowicz, and I. Moradi, 2023: Robustness of observing system simulation experiments. *Tellus*, **75A**, 309–333, <https://doi.org/10.16993/tellusa.3254>.
- Putman, W. M., and S.-J. Lin, 2007: Finite-volume transport on various cubed-sphere grids. *J. Comput. Phys.*, **227**, 55–78, <https://doi.org/10.1016/j.jcp.2007.07.022>.
- Reale, O., D. Achuthavarier, M. Fuentes, W. M. Putman, and G. Partyka, 2017: Tropical cyclones in the 7-km NASA global nature run for use in observing system simulation experiments. *J. Atmos. Oceanic Technol.*, **34**, 73–100, <https://doi.org/10.1175/JTECH-D-16-0094.1>.
- , E. L. McGrath-Spangler, W. McCarty, D. Holdaway, and R. Gelaro, 2018: Impact of adaptively thinned AIRS cloud-cleared radiances on tropical cyclone representation in a global data assimilation and forecast system. *Wea. Forecasting*, **33**, 909–931, <https://doi.org/10.1175/WAF-D-17-0175.1>.
- Rienecker, M. M., and Coauthors, 2008: The GEOS-5 data assimilation system—Documentation of versions 5.0.1, 5.1.0, and 5.2.0. NASA Tech. Memo. NASA/TM–2008-104606/Vol. 27, 118 pp., <https://ntrs.nasa.gov/citations/20120011955>.
- Schmit, T. J., J. Li, S. A. Ackerman, and J. J. Gurka, 2009: High-spectral- and high-temporal-resolution infrared measurements from geostationary orbit. *J. Atmos. Oceanic Technol.*, **26**, 2273–2292, <https://doi.org/10.1175/2009JTECHA1248.1>.
- Todling, R., and A. El Akkraoui, 2018: The GMAO hybrid ensemble-variational atmospheric data assimilation system: Version 2.0. NASA Tech. Memo. NASA/TM–2018-104606/Vol. 50, 184 pp., <https://gmao.gsfc.nasa.gov/pubs/docs/Todling1019.pdf>.
- Velden, C., and Coauthors, 2005: Recent innovations in deriving tropospheric winds from meteorological satellites. *Bull. Amer. Meteor. Soc.*, **86**, 205–224, <https://doi.org/10.1175/BAMS-86-2-205>.
- Wang, P., and Coauthors, 2015: Assimilation of thermodynamic information from advanced infrared sounders under partially cloudy skies for regional NWP. *J. Geophys. Res. Atmos.*, **120**, 5469–5484, <https://doi.org/10.1002/2014JD022976>.
- , J. Li, Z. Li, A. H. N. Lim, J. Li, and M. D. Goldberg, 2019: Impacts of observation errors on Hurricane forecasts when assimilating hyperspectral infrared sounder radiances in partially cloudy skies. *J. Geophys. Res. Atmos.*, **124**, 10802–10813, <https://doi.org/10.1029/2019JD031029>.
- , Z. Li, J. Li, and T. J. Schmit, 2021: Added-value of GEO-hyperspectral infrared radiances for local severe storm forecasts using the hybrid OSSE method. *Adv. Atmos. Sci.*, **38**, 1315–1333, <https://doi.org/10.1007/s00376-021-0443-1>.
- Wells, K. C., and Coauthors, 2020: Satellite isoprene retrievals constrain emissions and atmospheric oxidation. *Nature*, **585**, 225–233, <https://doi.org/10.1038/s41586-020-2664-3>.
- WMO, 2019: Vision for the WMO integrated global observing system in 2040. WMO Rep., 57 pp., https://library.wmo.int/doc_num.php?explnum_id=10278.
- Wu, W.-S., R. J. Purser, and D. F. Parrish, 2002: Three-dimensional variational analysis with spatially inhomogeneous covariances. *Mon. Wea. Rev.*, **130**, 2905–2916, [https://doi.org/10.1175/1520-0493\(2002\)130<2905:TDVAWS>2.0.CO;2](https://doi.org/10.1175/1520-0493(2002)130<2905:TDVAWS>2.0.CO;2).
- Yang, J., Z. Zhang, C. Wei, F. Lu, and Q. Guo, 2017: Introducing the new generation of Chinese geostationary weather satellites, Fengyun-4. *Bull. Amer. Meteor. Soc.*, **98**, 1637–1658, <https://doi.org/10.1175/BAMS-D-16-0065.1>.
- Zhou, D. K., and Coauthors, 2002: Thermodynamic product retrieval methodology and validation for NAST-I. *Appl. Opt.*, **41**, 6957–6967, <https://doi.org/10.1364/AO.41.006957>.
- Zhu, Y., and R. Gelaro, 2008: Observation sensitivity calculations using the adjoint of the Gridpoint Statistical Interpolation (GSI) analysis system. *Mon. Wea. Rev.*, **136**, 335–351, <https://doi.org/10.1175/MWR3525.1>.